

Contents lists available at ScienceDirect

Journal of Computational Physics

journal homepage: www.elsevier.com/locate/jcp



DGM-FD: A finite difference scheme based on the discontinuous Galerkin method applied to wave propagation

Anne M. Fernando ^{a,*}, Fang Q. Hu ^b

ARTICLE INFO

Article history: Received 8 July 2010 Received in revised form 12 January 2011 Accepted 3 March 2011 Available online 9 March 2011

Keywords: High order finite difference methods Wave propagation DGM

ABSTRACT

In this paper we formulate a numerical method that is high order with strong accuracy for numerical wave numbers, and is adaptive to non-uniform grids. Such a method is developed based on the discontinuous Galerkin method (DGM) applied to the hyperbolic equation, resulting in finite difference type schemes applicable to non-uniform grids. The schemes will be referred to as DGM-FD schemes. These schemes inherit naturally some features of the DGM, such as high-order approximations, applicability to non-uniform grids and super-accuracy for wave propagations. Stability of the schemes with boundary closures is investigated and validated. Proposed scheme is demonstrated by numerical examples including the linearized acoustic waves and solutions of non-linear Burger's equation and the flat-plate boundary layer problem. For non-linear equations, proposed flux finite difference formula requires no explicit upwind and downwind split of the flux. This is in contrast to existing upwind finite difference schemes in the literature.

© 2011 Elsevier Inc. All rights reserved.

1. Introduction

Accurate and efficient numerical wave approximation is important in many areas of study such as computational aero-acoustics (CAA). While dissipation and dispersion errors influence the accuracy of the method, efficiency can be assessed by computational cost and effective adaptability to different mesh structures. Finite difference and finite element methods are commonly used numerical schemes in CAA. Finite difference methods have the advantage of ease of use as well as high order convergence, but often require a uniform grid, and stable boundary closure can be non-trivial. High-order finite difference schemes optimized for such properties are widely used in CAA applications, such as compact schemes, Dispersion Relation Preserving (DRP) schemes and many others [5,11,19,20,26,32,33]. Finite element methods adapt well to different mesh structures but often become difficult to implement as the order of approximation increases. Discontinuous Galerkin method (DGM) is a finite element method that can use non-uniform grids and high-order basis functions. Recent studies have also shown that discontinuous Galerkin schemes have strong super-accuracy with low dissipation and dispersion errors for wave propagation problems [24,29].

This paper proposes a new finite difference type scheme, based on the discontinuous Galerkin method (DGM), that has strong numerical to exact wave number agreement, high order accuracy with stable boundary closure and adaptability to non-uniform grids [17]. DGM is chosen as the foundation of this new scheme for many reasons. DG methods are adept for handling complicated geometries and require relatively simple treatment of boundary conditions while maintaining high-order accuracy. Discontinuous Galerkin (DG) methods can also handle mesh adaptivity adjustments as refinements

E-mail address: amfernando@nsu.edu (A.M. Fernando).

^a Department of Mathematics, Norfolk State University, Norfolk, Virginia 23504, USA

^b Department of Mathematics and Statistics, Old Dominion University, Norfolk, Virginia 23529, USA

^{*} Corresponding author.

of the grid can be taken into account without concern about maintaining continuity [14]. DGM also performs well on non-uniform stencils, as studies on numerical reflections at a grid discontinuity reveal that the reflections are just the non-physical or spurious wave modes which dissipate quickly [24].

The original DG method was introduced by Reed and Hill in 1973 for solving the neutron transport equation [31]. A more formal analysis of DG as applied to ordinary differential equations was performed by LeSaint and Raviart where, if Δx is the grid spacing, they proved a rate of convergence of $(\Delta x)^p$ in one variable defined on Cartesian grids where p is the order of the basis functions [27]. On the issue of super-convergence, it was shown that the approximate solution of the DG method super-converges at the Gauss–Radau points [2,3,9]. Fourier analysis of DGM schemes has shown that the numerical eigenvalues are accurate to order 2p + 2 locally and therefore 2p + 1 globally for the decay of the evolution component of the numerical error [4,22,24]. Quadrature-free implementation of the Runge–Kutta discontinuous Galerkin (RKDG) was introduced in [6]. The extension of RKDG methods to general multi-dimensional systems was used in applications to the Euler equations of gas dynamics [7,8], and in a series of papers by Cockburn and Shu for numerically solving hyperbolic conservation laws [12,13,15,16]. Further review and discussion of properties of DGM for conservation laws was done by Flaherty et al. [18].

The new methods proposed in this work, DGM-FD schemes, are explicit and will be shown to possess many of the attractive features of the discontinuous Galerkin method including the ease of use on non-uniform grids, high-order accuracy, and low dissipation and low dispersion errors. It also applies directly to higher order derivatives.

In certain aspects, a recently emerged spectral differences (SD) method has some similarities to DGM-FD. SD makes use of Lagrange interpolating polynomials for a basis function expansion of the solution, u, and flux, f(u). However, while another recent method, Spectral Volumes (SV) in one dimension, is equivalent to SD [1]. In [34], it is shown that for one-dimension SV and DG are not equivalent. Therefore as DGM-FD, being equivalent to DG in one-dimension, is not equivalent to SV and therefore, not to SD. DGM-FD employs a weak formulation of finite elements to construct the numerical derivative of the flux, using Lax-Friedrichs formulation [24] to resolve the discontinuity at element boundaries inherent in DG formulation. The flux spatial derivative is composed of coefficients that are from inner products (with respect to L_2) of various combinations of the basis functions with themselves or their derivatives. For SD, the approach for finding the derivative of the flux polynomial could be a linear combination of the derivatives of the basis functions [1,28]. In the SD method, a linear combination of interpolating polynomials with the solution, u, at (p + 1) Gauss quadrature points as coefficients, is used to estimate the flux at (p + 2) Gauss-Lobatto points, including element boundaries [28]. While the solution and flux variables are collected at different sets of collocation points for SD, they are evaluated on the same grid points as DGM-FD.

This paper is organized as follows: in Section 2, a review of DGM is given leading to the semi-discrete form of the hyperbolic equation from which a finite difference formula for the first spatial derivative is constructed. Two grid structures, referred to as Grid Structure I and II, are considered in Sections 3 and 4. Stability of the schemes is analyzed in Section 5. Numerical wavenumber accuracy of the proposed schemes is studied in Section 6, followed by applications to the linearized Euler equations on non-uniform grids, the Burger's equations and the flat plate boundary layer problem governed by the Navier–Stokes equations in Section 7. Conclusions and comments are given in Section 8.

2. Formulation of derivative expression based on DGM

In this section, we present a finite difference type derivative formula that is based on the discontinuous Galerkin method. Consider the discontinuous Galerkin method, in one dimensional space, for

$$\frac{\partial u}{\partial t} + \frac{\partial f(u)}{\partial x} = 0 \tag{1}$$

with the spatial domain in x partitioned into elements $E_n = [s_{n-1}, s_n]$, n = 0, 1, ..., N. For the convenience of discussion, assume that the numerical solution and flux function for $x \in [s_{n-1}, s_n]$ are expanded as:

$$u_{h}^{n}(x,t) = \sum_{\ell=0}^{p} u_{n\ell}(t)\phi_{\ell}^{n}(\xi)$$
 (2)

$$f_h^n(\mathbf{x},t) = \sum_{\ell=0}^p f_{n\ell}(t)\phi_\ell^n(\xi) \tag{3}$$

where $x = \frac{1}{2}(s_{n-1} + s_n) + \frac{h_n}{2}\xi$, $h_n = s_n - s_{n-1}$, and $\phi_\ell^n(\xi)$ are the basis functions with order p on element E_n , in parametric coordinate ξ , where $-1 \leqslant \xi \leqslant 1$. We note that if $\phi_\ell^n(\xi)$ are chosen to be some nodal based Lagrange polynomials, the expansion coefficients will be the same as the nodal values of the numerical solution.

By a weak formulation in DGM, it is required that

$$\int_{s_{n-1}}^{s_n} \left[\frac{\partial u}{\partial t} + \frac{\partial f}{\partial x} \right] \phi_{\ell'}^n(x) dx = 0 \tag{4}$$

for $\ell'=0,1,\ldots,p$. Following an integration by parts and the change of variable given above that maps, for each n, $E_n=[s_{n-1},s_n]$ to [-1,1], we get

$$\frac{h_n}{2} \int_{-1}^{1} \frac{\partial u_h^n}{\partial t} \phi_{\ell'}^n(\xi) d\xi + f^*(s_n, t) \phi_{\ell'}^n(1) - f^*(s_{n-1}, t) \phi_{\ell'}^n(-1) - \int_{-1}^{1} f_h^n \frac{\partial \phi_{\ell'}^n}{\partial \xi} d\xi = 0$$
 (5)

for $\ell' = 0, 1, ..., p$, where f^* denotes the flux at the end points of the element. At the interface between two elements, or at element end points s_{n-1} and s_n , the flux vector f^* is not uniquely defined and a flux formula has to be supplied to complete the discretization process.

Here the Lax-Friedrichs flux formula, also known as the theta method, will be applied, namely

$$f^* = \frac{1}{2} [f^+ + f^- - \theta | \lambda | (u^+ - u^-)] \tag{6}$$

with λ being the largest eigenvalue in magnitude of the Jacobian of the flux evaluated at the element boundary point. The superscripts $^+$ and $^-$ refer to the values at the right and left of an element boundary, respectively, as shown in Fig. 1.

The semi-discrete expression (5) can then be written explicitly as

$$\begin{split} &\frac{h_{n}}{2} \sum_{\ell=0}^{p} \frac{\partial u_{n\ell}}{\partial t} \int_{-1}^{1} \phi_{\ell}^{n}(\xi) \phi_{\ell}^{n}(\xi) d\xi + \frac{1}{2} \left\{ \sum_{\ell=0}^{p} f_{n\ell} \phi_{\ell}^{n}(1) + \sum_{\ell=0}^{p} f_{(n+1)\ell} \phi_{\ell}^{n}(-1) + \theta |\lambda| \left(\sum_{\ell=0}^{p} u_{(n+1)\ell} \phi_{\ell}^{n}(-1) - \sum_{\ell=0}^{p} u_{n\ell} \phi_{\ell}^{n}(1) \right) \right\} \phi_{\ell}^{n}(1) \\ &- \frac{1}{2} \left\{ \sum_{\ell=0}^{p} f_{(n-1)\ell} \phi_{\ell}^{n}(1) + \sum_{\ell=0}^{p} f_{n\ell} \phi_{\ell}^{n}(-1) + \theta |\lambda| \left(\sum_{\ell=0}^{p} u_{n\ell} \phi_{\ell}^{n}(-1) - \sum_{\ell=0}^{p} u_{(n-1)\ell} \phi_{\ell}^{n}(1) \right) \right\} \phi_{\ell}^{n}(-1) \\ &- \sum_{\ell=0}^{p} f_{n\ell} \int_{-1}^{1} \phi_{\ell}^{n}(\xi) \frac{\partial \phi_{\ell}^{n}(\xi)}{\partial \xi} d\xi = 0 \end{split} \tag{7}$$

for $\ell' = 0, 1, \ldots, p$. In the above, θ , $0 \le \theta \le 1$, is a parameter that controls the upwinding effects, with $\theta = 0$ being a central scheme and $\theta = 1$ being the fully upwinded scheme. We note that Lax–Friedrichs formula is not the only scheme that could be used to complete the discretization process. A different flux formulation, however, might change the structure of the resulting derivative formula as we will see later.

To derive specific finite difference type schemes, we consider a special case that the basis functions are the same for all elements (except, perhaps, for those next to the boundary, as will be discussed later), denoted by

$$\phi_{\ell}^{n}(\xi) = P_{\ell}(\xi) \tag{8}$$

where $P_{\ell}(\xi)$, $\ell = 0,1,2,\ldots,p$, forms the basis set, and define matrices

$$\mathbf{Q} = \{q_{\ell'\ell}\} = \left\{ \int_{-1}^{1} P_{\ell} P_{\ell'} d\xi \right\}, \quad \mathbf{Q}' = \left\{ q_{\ell'\ell}' \right\} = \left\{ \int_{-1}^{1} P_{\ell} \frac{\partial P_{\ell'}}{\partial \xi} d\xi \right\}, \quad \mathbf{B}_{(a,b)} = \{b_{\ell'\ell}\} = \{P_{\ell'}(a)P_{\ell}(b)\}$$
(9)

and vectors

$$\vec{u}^n = \begin{bmatrix} u_{n0} \\ u_{n1} \\ \vdots \\ u_{np} \end{bmatrix}, \quad \vec{f}^n = \begin{bmatrix} f_{n0} \\ f_{n1} \\ \vdots \\ f_{np} \end{bmatrix}$$

Then, as given in [24], the semi-discrete equation (7) can be written as

$$\begin{split} &\frac{h_n}{2} \mathbf{Q} \frac{\partial \vec{u}^n}{\partial t} - \frac{1}{2} \mathbf{B}_{(-1,1)} \vec{f}^{n-1} + \left[\frac{1}{2} \mathbf{B}_{(1,1)} - \frac{1}{2} \mathbf{B}_{(-1,-1)} - \mathbf{Q}' \right] \vec{f}^n + \frac{1}{2} \mathbf{B}_{(1,-1)} \vec{f}^{n+1} \\ &+ \frac{\theta}{2} |\lambda| \left\{ -\mathbf{B}_{(-1,1)} \vec{u}^{n-1} + \left[\mathbf{B}_{(1,1)} + \mathbf{B}_{(-1,-1)} \right] \vec{u}^n - \mathbf{B}_{(1,-1)} \vec{u}^{n+1} \right\} = 0 \end{split}$$

or

$$\frac{h_n}{2} \mathbf{Q} \frac{\partial \vec{u}^n}{\partial t} + \mathbf{M}_{-} \vec{f}^{n-1} + \mathbf{M}_{0} \vec{f}^n + \mathbf{M}_{+} \vec{f}^{n+1} + \theta |\lambda| \left\{ \mathbf{M}_{-} \vec{u}^{n-1} + \mathbf{N}_{0} \vec{u}^n - \mathbf{M}_{+} \vec{u}^{n+1} \right\} = 0 \tag{10}$$

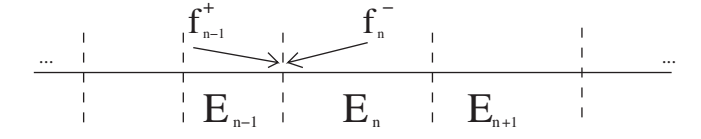


Fig. 1. A description of the location of f^+ , f^- on an a grid with element boundary.

where it is found that

$$\mathbf{M}_{-} = -\frac{1}{2}\mathbf{B}_{(-1,1)} \tag{11}$$

$$\boldsymbol{M}_0 = \frac{1}{2}\boldsymbol{B}_{(1,1)} - \frac{1}{2}\boldsymbol{B}_{(-1,-1)} - \boldsymbol{Q}' \tag{12}$$

$$\mathbf{M}_{+} = \frac{1}{2} \mathbf{B}_{(1,-1)} \tag{13}$$

$$\mathbf{N}_0 = \frac{1}{2} \mathbf{B}_{(1,1)} + \frac{1}{2} \mathbf{B}_{(-1,-1)} \tag{14}$$

Now by applying $\frac{2}{h_n} \mathbf{Q}^{-1}$, which is assumed to exist as the basis functions span the polynomial test and trial spaces, to (10) to get:

$$\frac{\partial \vec{\mathbf{u}}^n}{\partial t} + \frac{2}{h_n} \left\{ \overline{\mathbf{M}}_{-} \vec{\mathbf{f}}^{n-1} + \overline{\mathbf{M}}_{0} \vec{\mathbf{f}}^n + \overline{\mathbf{M}}_{+} \vec{\mathbf{f}}^{n+1} + \theta |\lambda| (\overline{\mathbf{M}}_{-} \vec{\mathbf{u}}^{n-1} + \overline{\mathbf{N}}_{0} \vec{\mathbf{u}}^n - \overline{\mathbf{M}}_{+} \vec{\mathbf{u}}^{n+1}) \right\} = \mathbf{0}$$
(15)

where

$$\overline{M}_- = Q^{-1}M_-, \quad \overline{M}_+ = Q^{-1}M_+, \quad \overline{M}_0 = Q^{-1}M_0, \quad \overline{N}_0 = Q^{-1}N_0$$

By comparing the original PDE (1) with the discretized version in (15) it is clear that we get the following discretization formula for the spatial derivative of the flux \vec{f}^n as

$$\frac{\partial \vec{f}^n}{\partial x} = \frac{2}{h_n} \left\{ \overline{\mathbf{M}}_{-} \vec{\mathbf{f}}^{n-1} + \overline{\mathbf{M}}_{0} \vec{\mathbf{f}}^n + \overline{\mathbf{M}}_{+} \vec{\mathbf{f}}^{n+1} + \theta |\lambda| \left(\overline{\mathbf{M}}_{-} \vec{\mathbf{u}}^{n-1} + \overline{\mathbf{N}}_{0} \vec{\mathbf{u}}^n - \overline{\mathbf{M}}_{+} \vec{\mathbf{u}}^{n+1} \right) \right\}$$
(16)

In particular, if we let f = au, where a is a scalar, we can also get an expression for the spatial derivative of solution variable \vec{u}^n :

$$\frac{\partial \vec{\mathbf{u}}^n}{\partial \mathbf{x}} = \frac{2}{h_n} \left\{ (1 + \alpha \theta) \overline{\mathbf{M}}_{-} \vec{\mathbf{u}}^{\mathbf{n}-1} + (\overline{\mathbf{M}}_{\mathbf{0}} + \alpha \theta \overline{\mathbf{N}}_{\mathbf{0}}) \vec{\mathbf{u}}^{\mathbf{n}} + (\mathbf{1} - \alpha \theta) \overline{\mathbf{M}}_{+} \vec{\mathbf{u}}^{\mathbf{n}+1} \right\}$$
(17)

where

$$\alpha = \operatorname{sign}(a) = \begin{cases} 1 & \text{if } a > 0 \\ -1 & \text{if } a < 0 \end{cases}$$

Depending on the choice for the sign of a, left (a < 0) and right (a > 0) biased difference formulas are formed. Here, θ is again, the upwinding factor. The formulation given above can be applied to any chosen family of basis functions $P_{\ell}(\xi)$. In particular, when the basis functions are chosen to be the Lagrange interpolating polynomials, the expansion coefficients $u_{n\ell}$ become the same as the nodal values of the numerical solution at the prescribed nodes. Expressions (16) and (17) then lead to spatial differential formulas for the flux and solution variable, like those in a finite difference method. Various finite-difference-like schemes can be derived by the formulas given in (16) and (17) based on particular choices on the distribution of nodal points. Two possibilities are detailed in the next two sections.

3. Grid Structure I

In this section, we present schemes with a distribution of nodal points that include the end points of the element. The nodal points in the local coordinates will be denoted by ξ_{ℓ} , $\ell = 0, 1, 2, \ldots, p$ and the globally ordered nodal points within

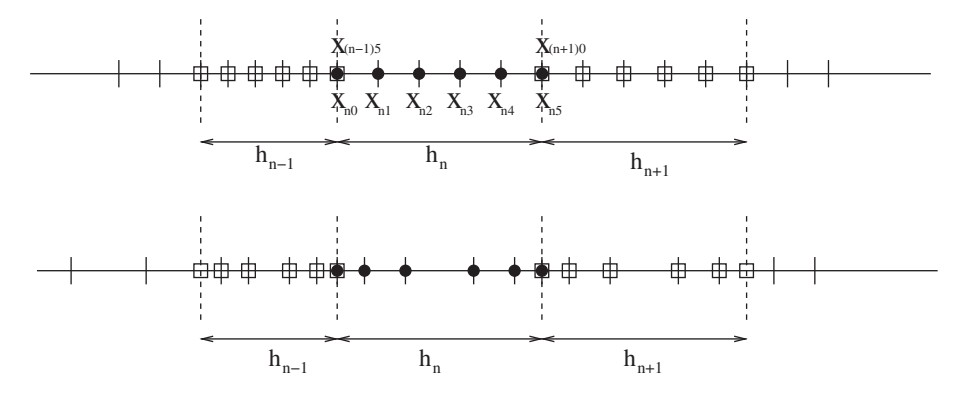


Fig. 2. Schematic of a finite difference grid partitioned into elements of length $h_n = p\Delta x$, where Δx is the grid size and p is the order of the basis functions. Top: uniform Δx and bottom: Chebychev–Labatto spacing.

element E_n will be denoted by $x_{n\ell}$, $\ell = 0, 1, 2, ..., p$, where p is the order of the basis functions. This will be referred to as Grid Structure I, see Fig. 2. Specifically, the nodal points on the transformed coordinate ξ , $-1 \le \xi \le 1$, can be

$$\xi_i = -1 + \frac{2i}{p}, \quad i = 0, 1, 2, \dots, p$$
 (18)

for a uniformly spaced grid, or

$$\xi_i = -\cos\left(\frac{i\pi}{p}\right), \quad i = 0, 1, 2, \dots, p \tag{19}$$

for a grid based on the Chebychev–Lobatto points [10]. After the nodal points have been chosen, the basis functions as given by (8) are

$$P_{\ell}(\xi) = \frac{\prod_{i=0, i \neq \ell}^{p} (\xi - \xi_{i})}{\prod_{i=0, i \neq \ell}^{p} (\xi_{\ell} - \xi_{i})}$$
(20)

Then the DGM-FD scheme can be derived by substituting (20) into formulation (16) or (17) where the matrices $\overline{\mathbf{M}}_{\mathbf{0}}$, $\overline{\mathbf{N}}_{\mathbf{0}}$, $\overline{\mathbf{M}}_{\pm}$ are computed according to (9) and (11)–(14).

In this grid structure, nodal points overlap at element end points, namely, $x_{np} \equiv x_{(n+1)0}$. Discontinuity of the solution at the end points is allowed thus, the solution is double valued at element end points.

We note that since element length, h_n , needs not be a constant from element to element, the grid which is made up of many such elements can be non-uniform, with no changes to scheme coefficients. This is a feature of the current scheme distinct from most existing finite difference schemes, where grid spacing is required to be constant.

3.1. Interior scheme

An example of a fifth-order (p = 5) scheme with uniformly distributed points (18) is shown below. Third and fourth order schemes are given in the appendix. By (16) the difference formula for the flux function on a set of six grid points is of the form

$$\frac{\partial}{\partial x} \begin{bmatrix} f_{n0} \\ f_{n1} \\ f_{n2} \\ f_{n3} \\ f_{n4} \\ f_{n5} \end{bmatrix} = \frac{2}{\mathbf{h}_{n}} \overline{\mathbf{M}}_{-} \begin{bmatrix} f_{(n-1)0} \\ f_{(n-1)1} \\ f_{(n-1)2} \\ f_{(n-1)3} \\ f_{(n-1)4} \\ f_{(n-1)5} \end{bmatrix} + \frac{2}{\mathbf{h}_{n}} \overline{\mathbf{M}}_{0} \begin{bmatrix} f_{n0} \\ f_{n1} \\ f_{n2} \\ f_{n3} \\ f_{n4} \\ f_{n5} \end{bmatrix} + \frac{2}{\mathbf{h}_{n}} \overline{\mathbf{M}}_{+} \begin{bmatrix} f_{(n+1)0} \\ f_{(n+1)1} \\ f_{(n+1)2} \\ f_{(n+1)3} \\ f_{(n+1)4} \\ f_{(n+1)5} \end{bmatrix} + \frac{2}{\mathbf{h}_{n}} \theta |\lambda| \overline{\mathbf{M}}_{-} \begin{bmatrix} u_{n0} \\ u_{n1} \\ u_{n2} \\ u_{n1} \\ u_{n2} \\ u_{n1} \\ u_{n4} \\ u_{n5} \end{bmatrix} - \frac{2}{\mathbf{h}_{n}} \theta |\lambda| \overline{\mathbf{M}}_{+} \begin{bmatrix} u_{(n+1)0} \\ u_{(n+1)1} \\ u_{(n+1)2} \\ u_{(n+1)3} \\ u_{(n+1)4} \\ u_{(n+1)5} \end{bmatrix}$$

$$(21)$$

For a uniformly spaced nodal distribution, given by (18), the coefficient matrices can be easily computed by (11)–(14). They are

$$\begin{split} \overline{\boldsymbol{M}}_{-} &= \begin{bmatrix} 0 & 0 & 0 & 0 & 0 & -9 \\ 0 & 0 & 0 & 0 & 0 & \frac{7611}{6250} \\ 0 & 0 & 0 & 0 & 0 & \frac{7611}{6250} \\ 0 & 0 & 0 & 0 & 0 & \frac{1773}{6250} \\ 0 & 0 & 0 & 0 & 0 & \frac{1773}{6250} \\ 0 & 0 & 0 & 0 & 0 & \frac{57}{3125} \\ 0 & 0 & 0 & 0 & 0 & \frac{3}{2} \end{bmatrix}, \quad \overline{\boldsymbol{M}}_{0} = \begin{bmatrix} \frac{79}{24} & \frac{25}{2} & -\frac{25}{2} & \frac{25}{3} & -\frac{25}{8} & 2 \\ -\frac{5368}{3125} & -\frac{65}{24} & 5 & -\frac{5}{2} & \frac{5}{6} & -\frac{2669}{25000} \\ \frac{213763}{37500} & -\frac{5}{4} & -\frac{5}{6} & \frac{5}{2} & -\frac{5}{8} & \frac{13763}{37500} \\ -\frac{13763}{37500} & \frac{5}{8} & -\frac{5}{2} & \frac{5}{6} & \frac{5}{4} & -\frac{21317}{25000} \\ \frac{2669}{25000} & -\frac{5}{6} & \frac{5}{2} & -5 & \frac{65}{24} & \frac{5368}{3125} \\ -2 & \frac{25}{8} & -\frac{25}{3} & \frac{25}{22} & -\frac{25}{2} & -\frac{79}{22} \end{bmatrix} \end{split}$$

Since only values of end points at the neighboring elements are needed, the difference formula (21) can also be expressed more concisely as follows:

$$\frac{\partial}{\partial x} \begin{bmatrix} f_{n0} \\ f_{n1} \\ \vdots \\ f_{np} \end{bmatrix} = \frac{2}{h_n} \mathbf{D} \begin{bmatrix} f_{(n-1)p} \\ f_{n0} \\ f_{n1} \\ \vdots \\ f_{np} \\ f_{(n+1)0} \end{bmatrix} + \frac{2}{h_n} \theta |\lambda| \mathbf{D}' \begin{bmatrix} u_{(n-1)p} \\ u_{n0} \\ u_{n1} \\ \vdots \\ u_{np} \\ u_{(n+1)0} \end{bmatrix}$$
(22)

Here p=5 for the current example. The entries for \mathbf{D} and \mathbf{D}' matrices can easily be found according to (21). Specifically that the first column of \mathbf{D} is the last column of $\overline{\mathbf{M}}_-$, its last column is the first one from $\overline{\mathbf{M}}_+$, with the remaining entries being from $\overline{\mathbf{M}}_0$. Likewise, the first column of \mathbf{D}' is also the last one from $\overline{\mathbf{M}}_-$ and therefore identical to the first column of \mathbf{D} , the last column is the opposite of the first one from $\overline{\mathbf{M}}_+$ and therefore the opposite of the last column from \mathbf{D} , and the middle columns are identical to those in $\overline{\mathbf{N}}_0$. \mathbf{D} and \mathbf{D}' for the current scheme are given explicitly below:

$$\mathbf{D} = \begin{bmatrix} -9 & \frac{79}{24} & \frac{25}{2} & -\frac{25}{2} & \frac{25}{3} & -\frac{25}{8} & 2 & -\frac{3}{2} \\ \frac{7611}{6250} & -\frac{5368}{3125} & -\frac{65}{24} & 5 & -\frac{5}{2} & \frac{5}{6} & -\frac{2669}{25000} & -\frac{57}{3125} \\ -\frac{2274}{3175} & \frac{21317}{25000} & -\frac{5}{4} & -\frac{5}{6} & \frac{5}{2} & -\frac{5}{8} & \frac{13763}{37500} & -\frac{1773}{6250} \\ \frac{1773}{6250} & -\frac{13763}{37500} & \frac{5}{8} & -\frac{5}{2} & \frac{5}{6} & \frac{5}{4} & -\frac{21317}{25000} & \frac{2274}{3125} \\ \frac{57}{3125} & \frac{2669}{25000} & -\frac{5}{6} & \frac{5}{2} & -5 & \frac{65}{24} & \frac{5348}{3125} & -\frac{761}{6250} \\ \frac{3}{2} & -2 & \frac{25}{8} & -\frac{25}{3} & \frac{25}{2} & -\frac{25}{2} & -\frac{79}{22} & 9 \end{bmatrix}$$
 and
$$\mathbf{D}' = \begin{bmatrix} -9 & 9 & 0 & 0 & 0 & 0 & -\frac{3}{2} & \frac{3}{2} & -\frac{3}{2} & 0 \\ \frac{7611}{6250} & -\frac{7611}{6250} & 0 & 0 & 0 & 0 & -\frac{57}{3125} & \frac{57}{3125} \\ -\frac{2274}{6250} & -\frac{2274}{3175} & \frac{2274}{3125} & 0 & 0 & 0 & 0 & 0 & \frac{2274}{3125} & -\frac{2274}{3125} \\ \frac{57}{3125} & -\frac{57}{3125} & 0 & 0 & 0 & 0 & 0 & -\frac{7611}{6250} & \frac{7611}{6250} \\ \frac{3}{2} & -\frac{3}{2} & 0 & 0 & 0 & 0 & 9 & -9 \end{bmatrix}$$

It is also straight forward to derive the difference formula for solution variable u from (22), which yields

$$\frac{\partial}{\partial x} \begin{bmatrix} u_{n0} \\ u_{n1} \\ \vdots \\ u_{np} \end{bmatrix} = \frac{2}{h_n} [\mathbf{D} \pm \theta \mathbf{D}'] \begin{bmatrix} u_{(n-1)p} \\ u_{n0} \\ u_{n1} \\ \vdots \\ u_{np} \\ u_{(n+1)0} \end{bmatrix}$$
(23)

where a + or - sign is taken when $\frac{\partial f}{\partial u} > 0$ or $\frac{\partial f}{\partial u} < 0$, respectively, giving a left or right biased scheme.

3.2. Boundary closures

Forming a boundary closure is accomplished by assuming that variables in the boundary grid point are single-valued, as illustrated in Fig. 3. Grid points near the boundary are show in Fig. 3 where a left boundary is closed one order down for added stability [11]. To illustrate the boundary schemes, let element index be n = 0 for the element at the left boundary. Using the formulation outlined in (23) as an example, the left boundary closure involves adjusting the coefficients for the first collocation point at the boundary of the first element and by adding the first two columns of the **D** and **D**' matrices thus created. This produces boundary closure matrices, \mathbf{D}^{cl} and $\mathbf{D}^{',cl}$:

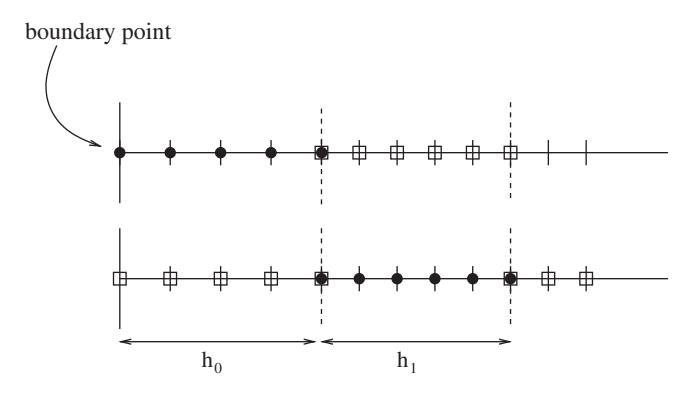


Fig. 3. Schematic of grids at the boundary, p = 4.

$$\mathbf{p}^{cl} = \begin{bmatrix} -\frac{25}{6} & 8 & -6 & \frac{8}{3} & -\frac{7}{4} & \frac{5}{4} \\ -\frac{1}{2} & -\frac{5}{3} & 3 & -1 & \frac{511}{1536} & -\frac{85}{512} \\ \frac{1}{6} & -\frac{4}{3} & 0 & \frac{4}{3} & -\frac{61}{96} & \frac{15}{32} \\ -\frac{1}{6} & 1 & -3 & \frac{5}{3} & \frac{741}{512} & -\frac{485}{512} \\ \frac{1}{2} & -\frac{8}{3} & 6 & -8 & -\frac{25}{12} & \frac{24}{3} \end{bmatrix} \text{ and } \mathbf{p}^{\prime,cl} = \begin{bmatrix} 0 & 0 & 0 & 0 & \frac{5}{4} & -\frac{5}{4} \\ 0 & 0 & 0 & 0 & -\frac{85}{512} & \frac{85}{512} \\ 0 & 0 & 0 & 0 & \frac{15}{32} & -\frac{15}{32} \\ 0 & 0 & 0 & 0 & -\frac{485}{485} & \frac{485}{512} \\ 0 & 0 & 0 & 0 & \frac{25}{4} & -\frac{25}{4} \end{bmatrix}$$

With which the derivative formula for solution variable would be

$$\frac{\partial}{\partial \mathbf{x}} \begin{bmatrix} u_{n0} \\ u_{n1} \\ \vdots \\ u_{n(p-1)} \end{bmatrix} = \frac{2}{h_n} [\mathbf{D}^{cl} \pm \theta \mathbf{D}^{\prime, cl}] \begin{bmatrix} u_{n0} \\ u_{n1} \\ \vdots \\ u_{n(p-1)} \\ u_{(n+1)0} \end{bmatrix}$$
(24)

for n = 0 at the left boundary.

Closure for the right side follows similarly. The above scheme gives coefficients for computing a spatial derivative and these can be used to incorporate forcing terms or boundary conditions as applicable. We note that, when the boundary value is given, the derivative formula for the boundary point may not be used.

4. Grid Structure II

In this section, a second choice for the nodal points is studied, where nodal points lie inside the element. By choosing nodal points all in the interior of the element, it is possible to generate a grid system without double-valued nodes as shown in Fig. 4. In this case, the nodal points on the transformed coordinate ξ , $-1 \leqslant \xi \leqslant 1$, are

$$\xi_i = -\frac{p}{p+1} + \frac{2i}{p+1}, \quad i = 0, 1, 2, \dots, p$$
 (25)

for a uniformly spaced grid or

$$\xi_i = -\cos\left(\frac{(2i+1)\pi}{2p+2}\right), \quad i = 0, 1, 2, \dots, p$$
 (26)

for a grid based on Chebychev-Gauss points [10].

This will be referred to as Grid Structure II. Since this scheme does not require double grid points, it resembles, more closely, a traditional finite difference scheme, when uniform grids are used.

With the given choices of the grid points, the difference formula can again be easily derived by substituting (20) into formulation (16) or (17) where the matrices are computed according to (9) and (11)–(14).

4.1. Interior scheme

A fourth-order (p = 4) scheme is given below as an example. The difference formula by (16) for a set of five grid points, as illustrated in Fig. 4, is of the form

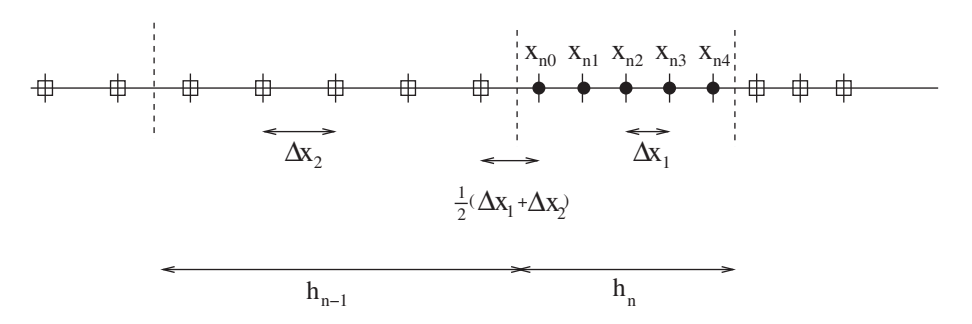


Fig. 4. Schematic of a finite difference non-uniform grid partitioned into elements of length $h_n = (p+1)\Delta x$, where Δx is the grid size and p is the order of the basis functions.

$$\frac{\partial}{\partial x} \begin{bmatrix} f_{n0} \\ f_{n1} \\ f_{n2} \\ f_{n3} \\ f_{n4} \end{bmatrix} = \frac{2}{\mathbf{h}_{n}} \overline{\mathbf{M}}_{-} \begin{bmatrix} f_{(n-1)0} \\ f_{(n-1)1} \\ f_{(n-1)2} \\ f_{(n-1)3} \\ f_{(n-1)4} \end{bmatrix} + \frac{2}{\mathbf{h}_{n}} \overline{\mathbf{M}}_{0} \begin{bmatrix} f_{n0} \\ f_{n1} \\ f_{n2} \\ f_{n3} \\ f_{n4} \end{bmatrix} + \frac{2}{\mathbf{h}_{n}} \overline{\mathbf{M}}_{+} \begin{bmatrix} f_{(n+1)0} \\ f_{(n+1)1} \\ f_{(n+1)2} \\ f_{(n+1)3} \\ f_{(n+1)4} \end{bmatrix} + \frac{2}{\mathbf{h}_{n}} \theta |\lambda| \overline{\mathbf{M}}_{-} \begin{bmatrix} u_{(n-1)0} \\ u_{(n-1)1} \\ u_{(n-1)2} \\ u_{(n-1)3} \\ u_{(n-1)4} \end{bmatrix} + \frac{2}{\mathbf{h}_{n}} \theta |\lambda| \overline{\mathbf{N}}_{0} \begin{bmatrix} u_{n0} \\ u_{n1} \\ u_{n2} \\ u_{n3} \\ u_{n4} \end{bmatrix} - \frac{2}{\mathbf{h}_{n}} \theta |\lambda| \overline{\mathbf{M}}_{+} \begin{bmatrix} u_{(n+1)0} \\ u_{(n+1)1} \\ u_{(n+1)2} \\ u_{(n+1)3} \\ u_{(n+1)4} \end{bmatrix}$$

$$(27)$$

By using (25) and (20) as the nodal points and basis functions, the coefficient matrices are readily computed by (11)–(14) as follows:

$$\overline{\mathbf{M}}_{\mathbf{0}} = \begin{bmatrix} \frac{-29141}{102400} & \frac{37467}{25600} & \frac{-786807}{256000} & \frac{87423}{25600} & \frac{-262269}{102400} \\ \frac{-22379}{102400} & \frac{-28773}{25600} & \frac{604233}{256000} & \frac{-67137}{25600} & \frac{201411}{20400} \\ \frac{-525}{256000} & \frac{-256000}{256000} & \frac{256000}{256000} & \frac{102400}{25600} \\ \frac{-3941}{102400} & \frac{50675}{25600} & \frac{-2835}{256000} & \frac{10724}{25600} & \frac{4096}{25600} \\ \frac{-3941}{102400} & \frac{5067}{25600} & \frac{-106407}{256000} & \frac{11823}{25600} & \frac{-35469}{102400} \\ \frac{12299}{102400} & \frac{-15813}{256000} & \frac{332073}{256000} & \frac{-36897}{102400} & \frac{110691}{102400} \\ \frac{-33669}{12800} & \frac{14153}{25000} & \frac{3117}{25000} & \frac{2149}{25000} & \frac{-13693}{25600} \\ \frac{-33699}{138400} & \frac{14153}{6400} & \frac{3117}{3200} & \frac{2149}{25600} & \frac{-1895}{25600} \\ \frac{13693}{38400} & \frac{-2149}{6400} & \frac{-3117}{3200} & \frac{-14153}{3200} & \frac{33669}{38400} \\ \frac{13693}{38400} & \frac{-2149}{6400} & \frac{-3117}{3200} & \frac{-14153}{3200} & \frac{33669}{38400} \\ \frac{-9479}{12800} & \frac{-8227}{16000} & \frac{5007}{6400} & \frac{-38491}{38400} \\ \frac{-9479}{10240} & \frac{-32560}{2560} & \frac{128000}{25600} & \frac{2560}{2048} \\ \frac{-19747}{10240} & \frac{2560}{2560} & \frac{128000}{25600} & \frac{2560}{2048} \\ \frac{-19747}{10240} & \frac{2560}{2560} & \frac{128000}{25600} & \frac{25600}{10240} \\ \frac{-2625}{2048} & \frac{-1125}{512} & \frac{2835}{10240} & \frac{-1125}{5260} & \frac{2625}{2048} \\ \frac{-10240}{25600} & \frac{256000}{256000} & \frac{25600}{25600} & \frac{102400}{102400} \\ \frac{-3649}{25600} & \frac{-332073}{25600} & \frac{15813}{2560} & \frac{-12299}{10240} \\ \frac{-1631}{20400} & \frac{-5}{256000} & \frac{256000}{256000} & \frac{25600}{102400} & \frac{102400}{25600} \\ \frac{-26269}{26269} & \frac{-87423}{25600} & \frac{256000}{256000} & \frac{25600}{256000} & \frac{102400}{102400} \\ \frac{-262269}{26269} & \frac{-87423}{25600} & \frac{256000}{256000} & \frac{25600}{256000} & \frac{102400}{25600} \\ \frac{-262269}{102400} & \frac{-87423}{25600} & \frac{256000}{256000} & \frac{25600}{256000} & \frac{102400}{25600} \\ \frac{-262269}{20249} & \frac{-87423}{25600} & \frac{256000}{256000} & \frac{25600}{256000} & \frac{102400}{25600} \\ \frac{-262269}{202499} & \frac{-87423}{25600} & \frac{256000}{256000} & \frac{256000}{256000} & \frac{25600}{25600} & \frac{102400}{20240}$$

Similarly, by letting f = au, where a is a scalar, a difference formula for any solution variable u can be obtained as

$$\frac{\partial}{\partial \mathbf{x}} \begin{bmatrix} u_{n0} \\ u_{n1} \\ u_{n2} \\ u_{n3} \\ u_{n4} \end{bmatrix} = \frac{2}{\mathbf{h}_{n}} (1 \pm \theta) \overline{\mathbf{M}}_{-} \begin{bmatrix} u_{(n-1)0} \\ u_{(n-1)1} \\ u_{(n-1)2} \\ u_{(n-1)3} \\ u_{(n-1)4} \end{bmatrix} + \frac{2}{\mathbf{h}_{n}} (\overline{\mathbf{M}}_{0} \pm \theta \overline{\mathbf{N}}_{0}) \begin{bmatrix} u_{n0} \\ u_{n1} \\ u_{n2} \\ u_{n3} \\ u_{n4} \end{bmatrix} + \frac{2}{\mathbf{h}_{n}} (\mathbf{1} - (\pm \theta)) \overline{\mathbf{M}}_{+} \begin{bmatrix} u_{(n+1)0} \\ u_{(n+1)1} \\ u_{(n+1)2} \\ u_{(n+1)3} \\ u_{(n+1)4} \end{bmatrix} \tag{28}$$

where a + or – sign should be taken when $\frac{\partial f}{\partial u} > 0$ or $\frac{\partial f}{\partial u} < 0$, respectively.

A central difference scheme is obtained by letting θ = 0 in (28). On the other hand, a choice of θ = 1 will yield upwind schemes with a stencil bias indicated by the coefficient sign of \pm preceding the θ .

It is also straight forward to show that the difference scheme is applicable to a grid of non-uniform spacings, provided that between grids of spacings Δx_1 and Δx_2 , there is a transitional grid of length $\frac{1}{2}(\Delta x_1 + \Delta x_2)$, i.e., the average of the two grid spacings, as shown in Fig. 4.

4.2. Boundary closures

For this grid structure, the nodal points are on the interior of the elements, and yet implementation of boundary conditions often requires the boundary to be on a collocation point. In such cases, the first and last element structures are adjusted so that each begins or ends on a nodal point. As the nodal points for the basis functions at the boundary element are adjusted to include the boundary point, as shown in Fig. 5, the basis polynomials generated by these nodal points will be different than the ones on the interior elements, and, therefore scheme coefficients need to be re-derived to complete the boundary

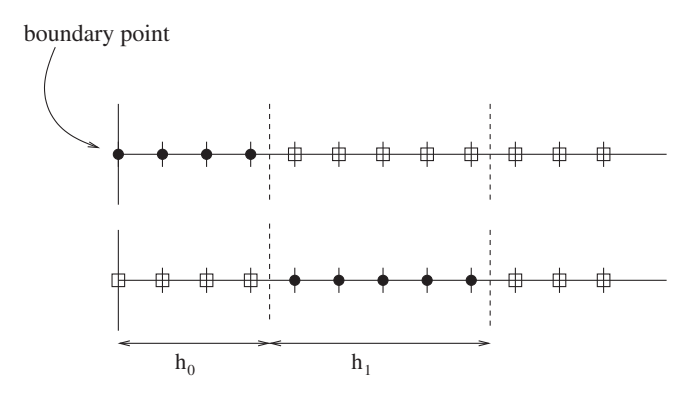


Fig. 5. Schematic of grids at the boundary, showing adjustment of element sizes. p = 4.

closures. In addition, the order of basis functions will be lowered for stability of the schemes [11]. The adjustment of element length with the lower order closure is also shown in Fig. 5.

Here are the general boundary closures, for any θ , for the first and last two elements to be used with the interior scheme shown in Section 4.1:

For the first element at the left boundary, \mathbf{E}_0 , the third order flux derivative formula is:

$$\frac{\partial}{\partial x} \begin{bmatrix} f_{00} \\ f_{01} \\ f_{02} \\ f_{03} \end{bmatrix} = \frac{2}{h_0} (\overline{\mathbf{M}}_{\mathbf{10}}^{\alpha} + \overline{\mathbf{M}}_{\mathbf{20}}^{\alpha}) \begin{bmatrix} f_{00} \\ f_{01} \\ f_{02} \\ f_{03} \end{bmatrix} + \frac{2}{\mathbf{h_0}} \overline{\mathbf{M}}_{+}^{\alpha} \begin{bmatrix} f_{10} \\ f_{11} \\ f_{12} \\ f_{13} \\ f_{14} \end{bmatrix} + \frac{2}{\mathbf{h_0}} \theta |\lambda| (\overline{\mathbf{M}}_{\mathbf{10}}^{\alpha} + \overline{\mathbf{M}}_{\mathbf{20}}^{\alpha}) \begin{bmatrix} u_{00} \\ u_{01} \\ u_{02} \\ u_{03} \end{bmatrix} - \frac{2}{\mathbf{h_0}} \theta |\lambda| \overline{\mathbf{M}}_{+}^{\alpha} \begin{bmatrix} u_{10} \\ u_{11} \\ u_{12} \\ u_{13} \\ u_{14} \end{bmatrix} \tag{29}$$

where

$$\overline{\boldsymbol{M}}_{\boldsymbol{10}}^{\alpha} = \begin{bmatrix} -4 & 0 & 0 & 0 \\ -\frac{24}{49} & 0 & 0 & 0 \\ \frac{4}{49} & 0 & 0 & 0 \\ -\frac{16}{49} & 0 & 0 & 0 \end{bmatrix}, \quad \overline{\boldsymbol{M}}_{\boldsymbol{20}}^{\alpha} = \begin{bmatrix} \frac{23}{48} & \frac{105}{16} & \frac{-77}{16} & \frac{133}{48} \\ -\frac{2209}{2352} & \frac{-23}{16} & \frac{48}{16} & \frac{-59}{48} \\ \frac{59}{2352} & \frac{-109}{112} & \frac{-47}{112} & \frac{631}{336} \\ \frac{11}{2352} & \frac{171}{112} & \frac{-383}{336} & \frac{463}{336} \end{bmatrix}$$

$$\overline{\boldsymbol{N}}_{\boldsymbol{0}}^{\alpha} = \begin{bmatrix} \frac{69}{16} & -\frac{21}{16} & \frac{35}{16} & -\frac{35}{16} \\ -\frac{489}{784} & \frac{9}{16} & -\frac{15}{16} & \frac{15}{16} \\ \frac{81}{784} & -\frac{87}{112} & \frac{145}{112} & -\frac{145}{112} \\ -\frac{51}{123} & -\frac{205}{205} & \frac{205}{205} \end{bmatrix}$$

$$\overline{\mathbf{M}}_{+}^{\alpha} = \begin{bmatrix} -\frac{315}{128} & \frac{105}{32} & -\frac{189}{64} & \frac{45}{32} & -\frac{35}{128} \\ \frac{135}{128} & \frac{-45}{32} & 81 & -\frac{135}{128} & \frac{15}{128} \\ \frac{135}{128} & \frac{32}{32} & 64 & \frac{224}{224} & \frac{128}{128} \\ -\frac{1305}{896} & \frac{435}{224} & -\frac{783}{448} & \frac{1305}{1568} & -\frac{145}{896} \\ \frac{1845}{896} & -\frac{615}{224} & \frac{1107}{448} & \frac{1568}{1568} & \frac{896}{896} \end{bmatrix}$$

For the second element at a left boundary, \mathbf{E}_1 , the 4th order flux derivative formula is:

$$\frac{\partial}{\partial x} \begin{bmatrix} f_{10} \\ f_{11} \\ f_{12} \\ f_{13} \\ f_{14} \end{bmatrix} = \frac{2}{h_{1}} \overline{\mathbf{M}}_{-}^{\beta} \begin{bmatrix} f_{00} \\ f_{01} \\ f_{02} \\ f_{03} \end{bmatrix} + \frac{2}{h_{1}} \overline{\mathbf{M}}_{0}^{\beta} \begin{bmatrix} f_{10} \\ f_{11} \\ f_{12} \\ f_{13} \\ f_{14} \end{bmatrix} + \frac{2}{h_{1}} \overline{\mathbf{M}}_{+}^{\beta} \begin{bmatrix} f_{20} \\ f_{21} \\ f_{22} \\ f_{23} \\ f_{24} \end{bmatrix} + \frac{2}{h_{1}} \theta |\lambda| \overline{\mathbf{M}}_{-}^{\beta} \begin{bmatrix} u_{00} \\ u_{01} \\ u_{02} \\ u_{03} \end{bmatrix} + \frac{2}{h_{1}} \theta |\lambda| \overline{\mathbf{N}}_{0}^{\beta} \begin{bmatrix} u_{10} \\ u_{11} \\ u_{12} \\ u_{13} \\ u_{14} \end{bmatrix} - \frac{2}{h_{1}} \theta |\lambda| \overline{\mathbf{M}}_{+}^{\beta} \begin{bmatrix} u_{20} \\ u_{21} \\ u_{22} \\ u_{23} \\ u_{24} \end{bmatrix} \tag{30}$$

where

$$\overline{\mathbf{M}}_{-}^{\beta} = \begin{bmatrix} \frac{4103}{6400} & -\frac{87423}{32000} & \frac{29141}{6400} & -\frac{29141}{6400} \\ -\frac{3197}{6400} & \frac{67137}{32000} & -\frac{6400}{6400} & \frac{6400}{6400} \\ \frac{75}{256} & -\frac{315}{256} & \frac{525}{256} & -\frac{525}{256} \\ \frac{563}{6400} & -\frac{11823}{32000} & \frac{3941}{6400} & \frac{3941}{6400} \\ -\frac{1757}{6400} & \frac{38897}{32000} & -\frac{12299}{6400} & \frac{12299}{6400} \end{bmatrix}$$

For the last two elements at a right boundary of the domain, we make use of anti-symmetry relationships for deriving the coefficients. More details are given in the appendix, including the coefficients for second and third order schemes.

5. Stability and super-accuracy properties

5.1. Stability

To study the stability of the scheme with boundary closure, we perform an eigenvalue analysis when the scheme is applied to the advection equation

$$\frac{\partial u}{\partial t} + \frac{\partial u}{\partial x} = 0, \quad x \in [0, 1]$$

with a given boundary condition at the left boundary, x = 0.

Let \mathbf{u}^h denote the global vector that contains all nodal values, except the one at the left boundary, then the semi-discrete equation for (31) can be written as

$$\frac{d\mathbf{u}^h}{dt} + \widetilde{\mathbf{D}}\mathbf{u}^h = \mathbf{s} \tag{32}$$

where \mathbf{s} is a source term created by the boundary condition. The discretization is stable if all of the eigenvalues of $\widetilde{\mathbf{D}}$ have positive real parts [11].

For Grid Structure I, as described in Section 3, the eigenvalues for the fifth-order scheme and the boundary closure presented in the previous sections with N = 30 elements are shown in Fig. 6, left. Stability of the eigenvalues is observed. The eigenvalue plots for a higher order scheme p = 9, with Chebychev–Lobatto points, show stability in Fig. 6, right, with N = 30. The eigenvalues were computed for many values of N, as low as N = 5 and as high as N = 200. The uniform grid shows an eigenvalue close to zero. This value is, like the others, is repeated and as N is increased and no new distinct eigenvalues appear. For p > 5, the scheme showed instability with a uniform grid. Therefore, for p > 5, Chebychev–Lobatto should be used.

For Grid Structure II, the eigenvalues for a third-order central scheme and a fourth order upwind scheme, with coefficients calculated as described in Section 4, are shown in Fig. 7 for N = 30. This was repeated for N = 5-200 for each p, where stability was confirmed for each case.

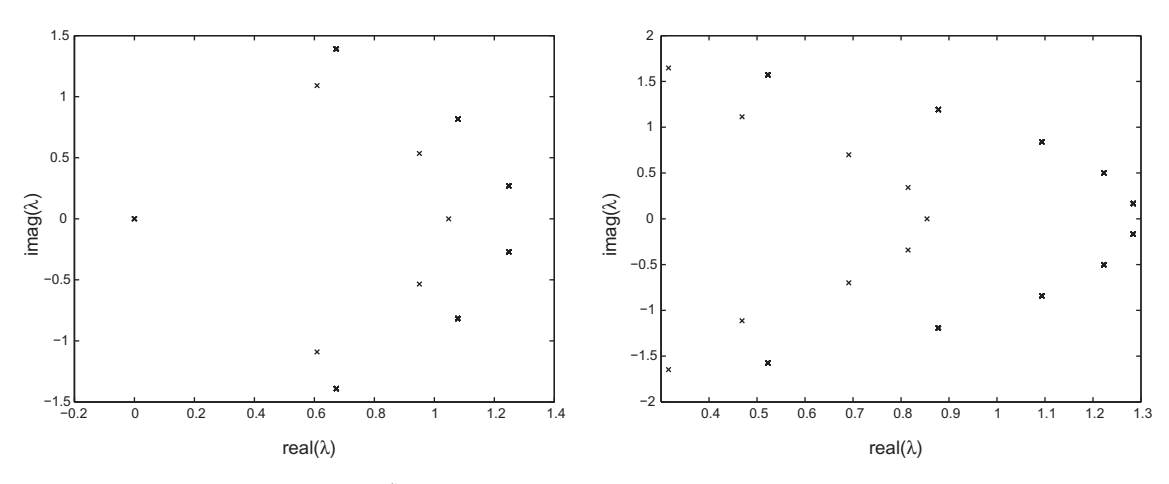


Fig. 6. Grid I: Left: eigenvalue λ of upwind scheme $\tilde{\mathbf{D}}_+$ (θ = 1). Eigenvalues are computed using N = 30 elements and p = 5. Right: Eigenvalues λ of upwind scheme $\tilde{\mathbf{D}}_+$ (θ = 1). Eigenvalues are computed using N = 30 elements, p = 9, and Chebychev–Labatto grid.

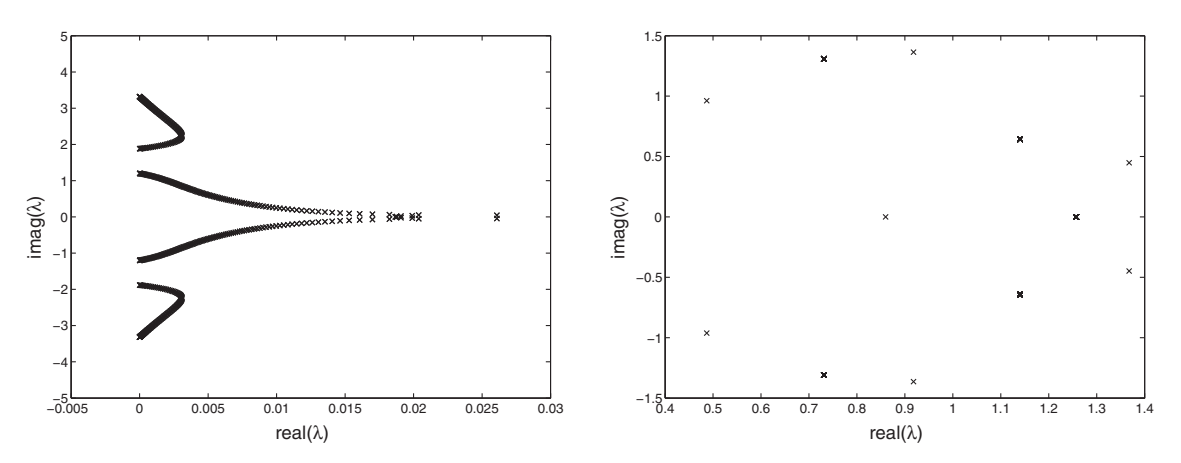


Fig. 7. Grid II: Left: eigenvalue λ of cental scheme $\tilde{\mathbf{D}}_0$ (θ = 0), p = 3; Right: eigenvalue λ of upwind scheme $\tilde{\mathbf{D}}_+$ (θ = 1), p = 4. Eigenvalues are computed using N = 30 elements.

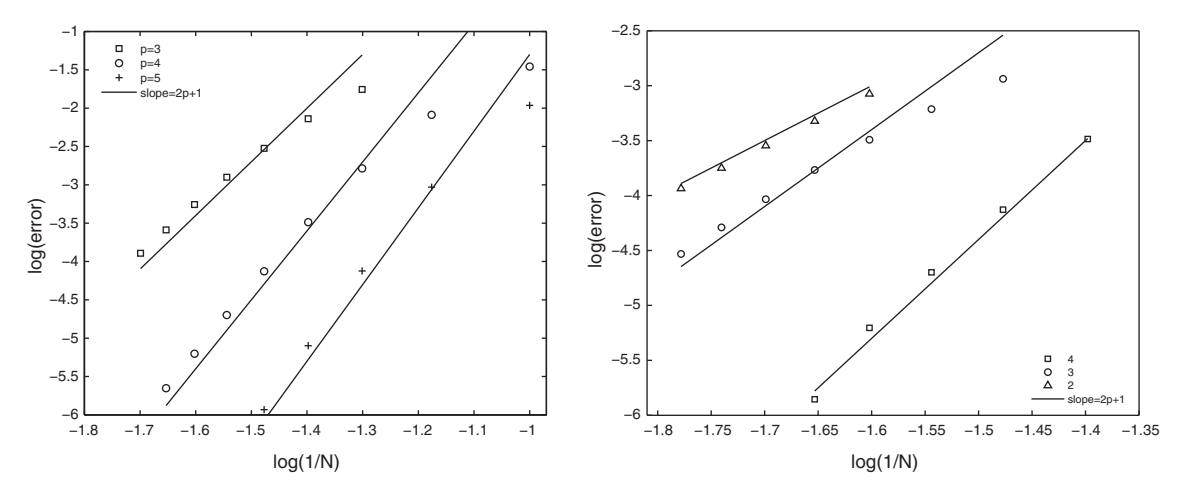


Fig. 8. mesh refinement study on the L2 norm of the difference between numerical solutions at t = 1, $u^h(x,1)$, and at t = 51, $u^h(x,51)$, left: Grid I p = 3,4,5 and right: Grid II p = 2,3,4 as indicated.

Table 1 Convergence rate data p = 3, 4, 5 for Grid Structure I.

θ = 1									
N	p = 3		p = 4		p = 5				
	Error	Rate	Error	Rate	Error	Rate			
25	7.2867E-3	3.9357	3.2545E-4	7.24280	7.9646E-6	10.0658			
30	2.9879E-3	4.8897	7.4643E-5	8.07610	1.1685E-6	10.5270			
35	1.2548E-3	5.6280	2.0024E-5	8.53570	2.2870E-7	10.5812			
40	5.5270E-4	6.1402	6.2671E-6	8.69908	_	_			
45	2.5812E-4	6.4644	2.2300E-6	8.77340	- -	_			
50	1.2800E-4	6.6575	_	_	_	_			

Table 2 Convergence rate data p = 2, 3, 4 for Grid Structure II.

N	p = 2		<i>p</i> = 3		p = 4	
	Error	Rate	Error	Rate	Error	Rate
25	-	_	_	_	3.2675E-4	_
30	_	-	1.1546E-2	-	7.4374E-5	8.1181
35	=	_	6.1181E-3	4.1199	1.9982E-5	8.5260
40	8.4202E-4	_	3.2212E-3	4.8040	6.2433E-6	8.7123
45	4.7652E-4	4.8335	1.7098E-3	5.3779	1.3989E-6	8.7984
50	2.8463E-4	4.8908	9.2492E-4	5.8315	=	_
55	1.7800E-4	4.9250	5.1363E-4	6.1708	-	-
60	1.1576E-4	4.9453	2.9398E-4	6.4133	_	_

5.2. Super-convergence

In recent Fourier analyses of the discontinuous Galerkin method, it was found that the propagation errors reduce at a super-convergent rate [4,24] To demonstrate the strong super-accuracy for wave propagation problems for DGM-FD, for both Grid Structures I and II, Eq. (31) is solved in a domain of $0 \le x \le 1$ with periodic boundary condition and an initial condition

$$u_0(x) = u(x,0) = e^{-\frac{\ln(2)}{0.0481^2} \left(x-\frac{1}{2}\right)^2}$$
(33)

First, using the upwind schemes given in Sections 3 and 4 with periodic closure, the numerical solution is calculated, from t = 0 to t = 51. The exact solution for the computational domain is the repeated initial condition at t = n where n is an integer. To demonstrate the super-accuracy for propagation errors, the solutions at t = 1 and t = 51 are compared and the L2 norm of the error, $\|u^h(x,51) - u^h(x,1)\|_2$, is shown in Fig. 8, Tables 1 and 2 as a function of total number of grid points in the grid refine studies for each scheme. We compare $u^h(x,51)$ to $u^h(x,1)$ rather than to the initial condition, as one advection period would dampen the non-physical mode of the numerical wave in the projected initial condition [24]. Convergence orders close to 5, 7 and 9 are observed even though the order of the basis function is p = 2,3,4, respectively, matching approximately the theoretical rate of convergence for the propagation error of order 2p + 1. This convergence is suggested for linear wave propagation specifically and it is unknown what kind of convergence can be seen in non-linear problems.

6. Numerical wave number accuracy

In this section, the numerical wave number accuracy of the DGM-FD method is examined and then compared to other finite difference schemes such as the DRP [32] and compact schemes [26]. Although the numerical wavenumbers of the DG method have been studied in the literature [4,22,24], we present a new way of computationally determining the numerical wavenumber accuracy. The method described below is easy to implement and quite general. It can be applied straightforwardly to many other numerical schemes.

First, the advection equation (31), is solved in a domain $-50 \le x \le 450$, using $\Delta x = 1$, with the initial condition

$$u_0(x) = e^{-\frac{\ln(2)}{3^2}x^2} \tag{34}$$

until a final time, e.g., T = 400. The exact solution at time T is

$$u_{\text{exact}}(x,T) = u_0(x-T) \tag{35}$$

The spatial Fourier transform of the exact solution is

$$\hat{u}_{exact}(k,T) = e^{-ikT}\hat{u}_0(k) \tag{36}$$

where a hat indicates the transformed function and k is the wave number. Here $\hat{u}_0(k)$ is the discrete Fourier transform of the initial condition on the computational grid.

Second, let the numerical solution at t = T be $u^*(x, T)$ and its discrete Fourier transform denoted by $\hat{u}^*(k, T)$. The numerical wavenumber k^* can be inferred from $\hat{u}^*(k, T)$ if we express it as

$$\hat{u}^*(k,T) = e^{-ik^*T}\hat{u}_0(k) \tag{37}$$

By comparing (37) with (36), an estimate of the difference $k^* - k$ can be obtained as

$$k^* - k = -\frac{\ln[\hat{u}^*(k, T)/\hat{u}_{exact}(k, T)]}{iT}.$$
(38)

6.1. Dissipation and dispersion errors of DGM-FD schemes

For both Grid Structures I and II, we first study the numerical wave number accuracy for the upwind (θ = 1) schemes for varying orders.

The numerical wave number accuracy, both for dispersion errors, $Real(k^* - k)$, and dissipation errors, $Imag(k^* - k)$, are shown in Figs. 9 and 10. The numerical solution becomes better resolved as the order, p, increases for the upwind scheme. In Fig. 9, the lowest value for p for Grid I of interest is assumed to be 3.

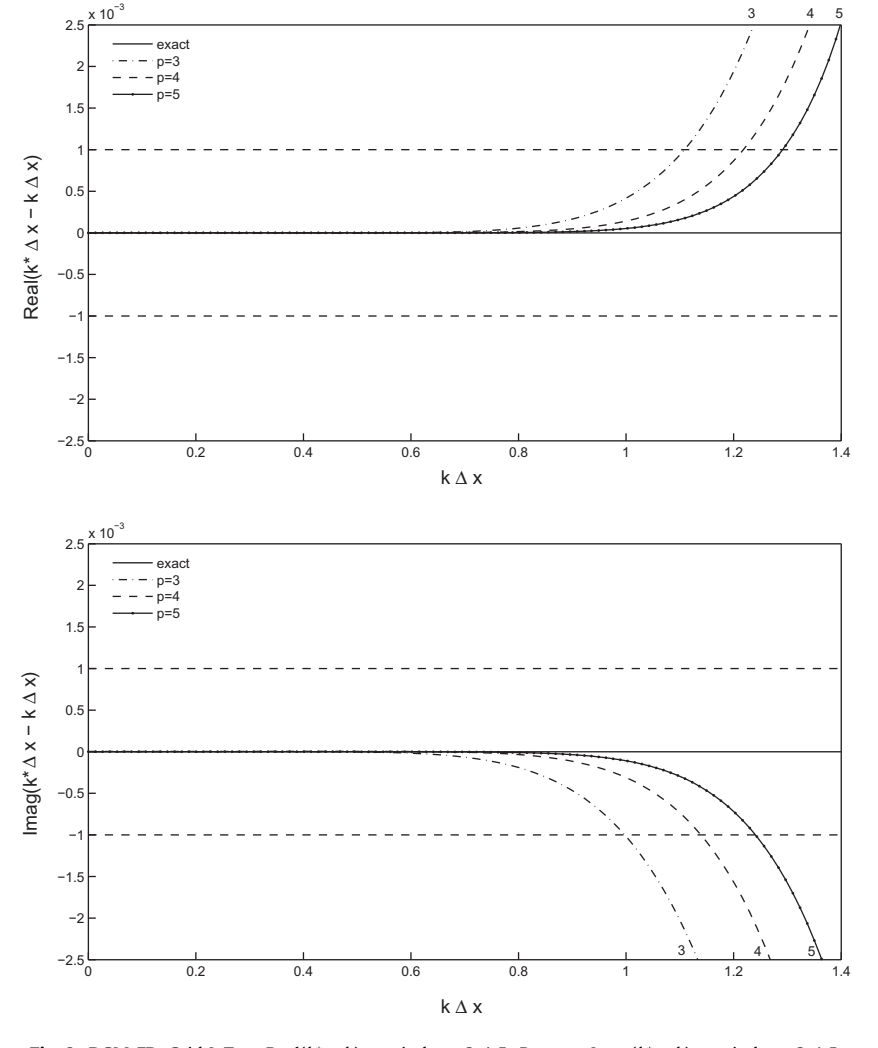


Fig. 9. DGM-FD, Grid I. Top: Real($k^* - k$) upwind, p = 3,4,5; Bottom: Imag($k^* - k$) upwind, p = 3,4,5.

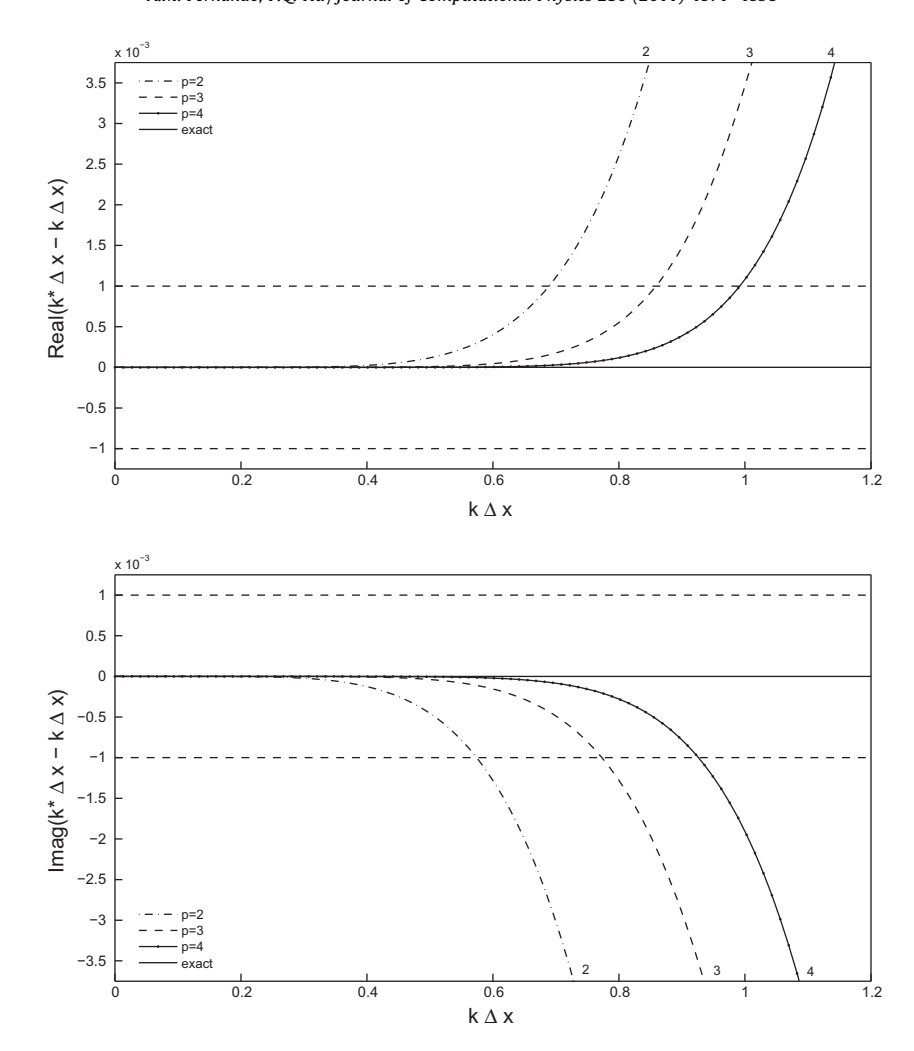


Fig. 10. DGM-FD, Grid II. Top: Real($k^* - k$) upwind, p = 2,3,4; Bottom: Imag($k^* - k$) upwind, p = 2,3,4.

For the central scheme (θ = 0) in Grid II, the numerical wave number accuracy is shown in Fig. 11. The accuracy for p = 3 appears to have a better numerical wave number resolution than for p = 4. The imaginary part of the numerical wave number is zero for the central schemes.

6.2. Comparison of DGM-FD with other FD schemes

Now we turn to comparing the performances of DGM-FD Grids I and II, with conventional finite difference schemes on the accuracy of numerical wave numbers. The advection equation (31) will be solved. First we compare their numerical solutions, then the numerical wave number accuracy followed by a comparison in their numerical wave number convergence rates.

In Fig. 12, the solution at t = 400, for DGM-FD Grid II of p = 4, the 4th and 6th order compact and the DRP schemes are shown with the initial condition given in (34). DGM-FD Grid II (p = 4) performs similarly with 6th order compact scheme and better than both 4th order and DRP.

In Fig. 13 the dispersion properties are examined. For the given tolerance of 10^{-3} , the difference between numerical and theoretical wave numbers, $k^* - k$, is comparable for DGM-FD, 6th order compact, and DRP, with $k\Delta x \le 1$. Fig. 14 shows the rate of convergence of the numerical wave number (slope in figures) for DGM-FD as higher than 4th, 6th and 8th order compact and DRP for the given range of Real($k\Delta x \le 1$).

We conclude this discussion of numerical wave number properties for Grid II with a recommendation for upwind parameter, θ for Grid II. With the central scheme (θ = 0), the results in Fig. 11 show no dissipation. With full upwinding (θ = 1) the results in Fig. 10 show better dispersion properties than for the central scheme, but with more numerical dissipation. We

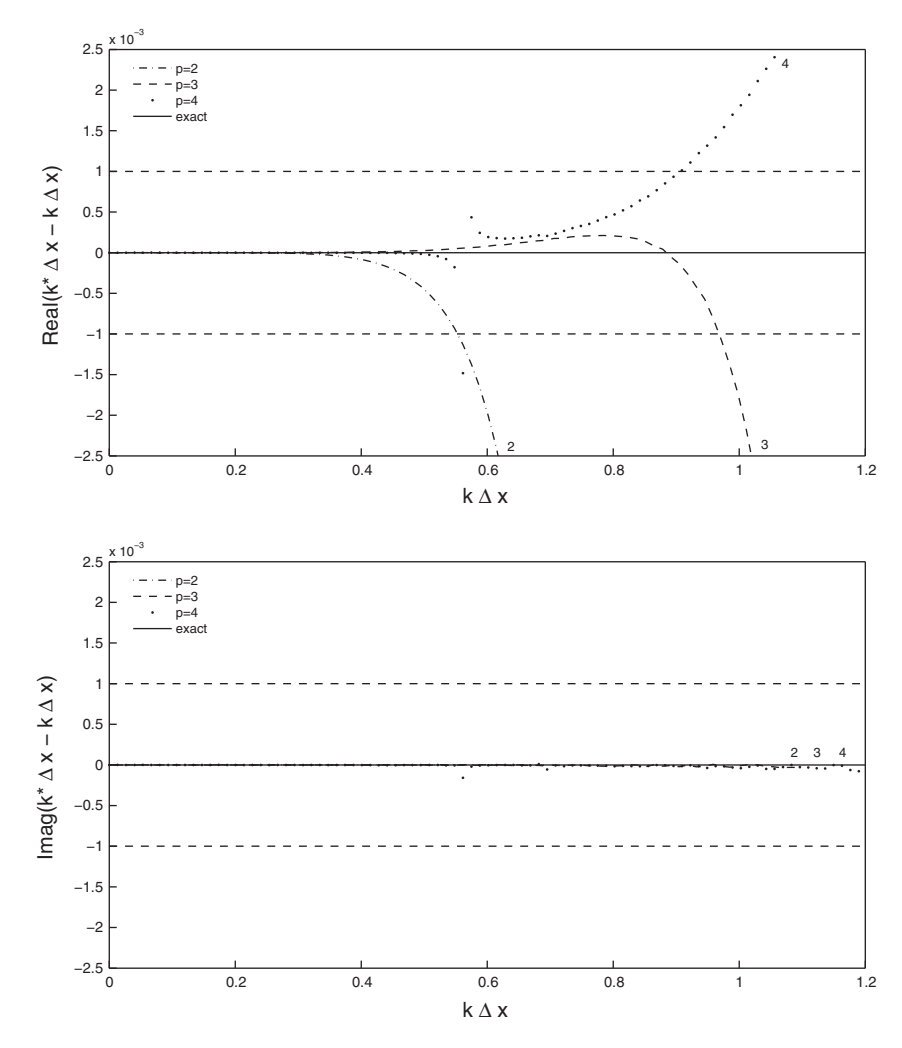


Fig. 11. DGM-FD, Grid II. Top: Real $(k^* - k)$ central, p = 2, 3, 4; Bottom: Imag $(k^* - k)$ central, p = 2, 3, 4.

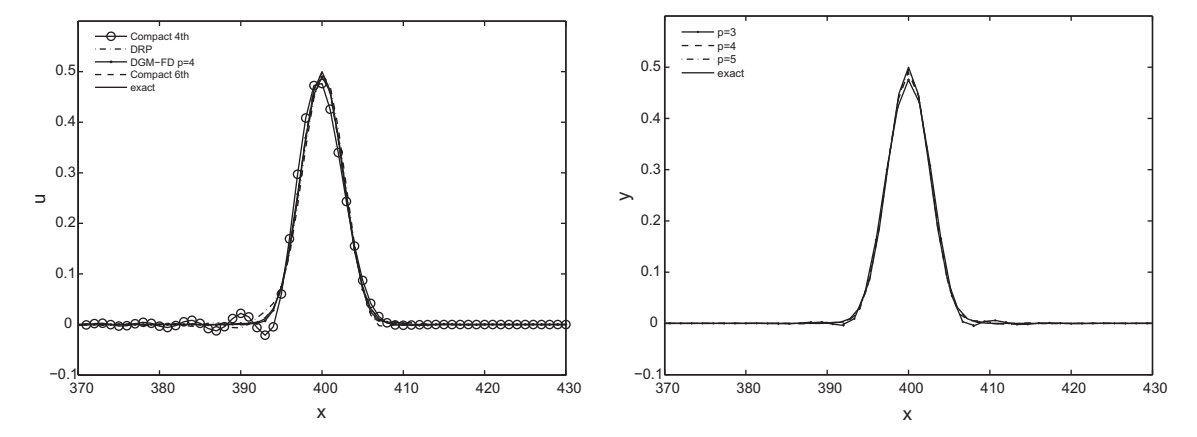


Fig. 12. Gaussian profile, left: Compact Schemes 4th, 6th order, DRP, and DGM-FD Grid II p = 4, DRP; right: DGM-FD Grid I p = 3,4,5.

look to balance both in Fig. 15. Numerical wave number errors for θ = 0.50, 0.75 and 1 are plotted. By these results, θ = 0.75 is recommended as the dispersion and dissipation errors are of similar magnitude.

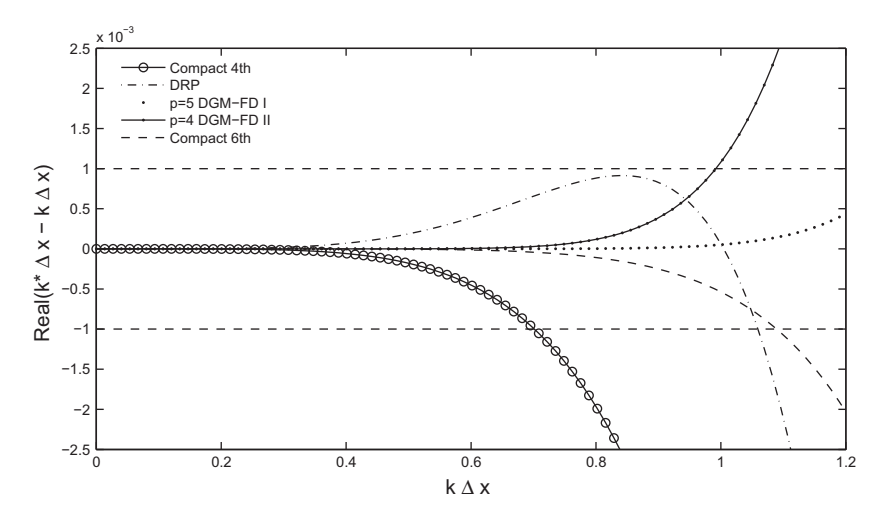


Fig. 13. Real($k^* - k$) compact, DRP DGM-FD I, II.

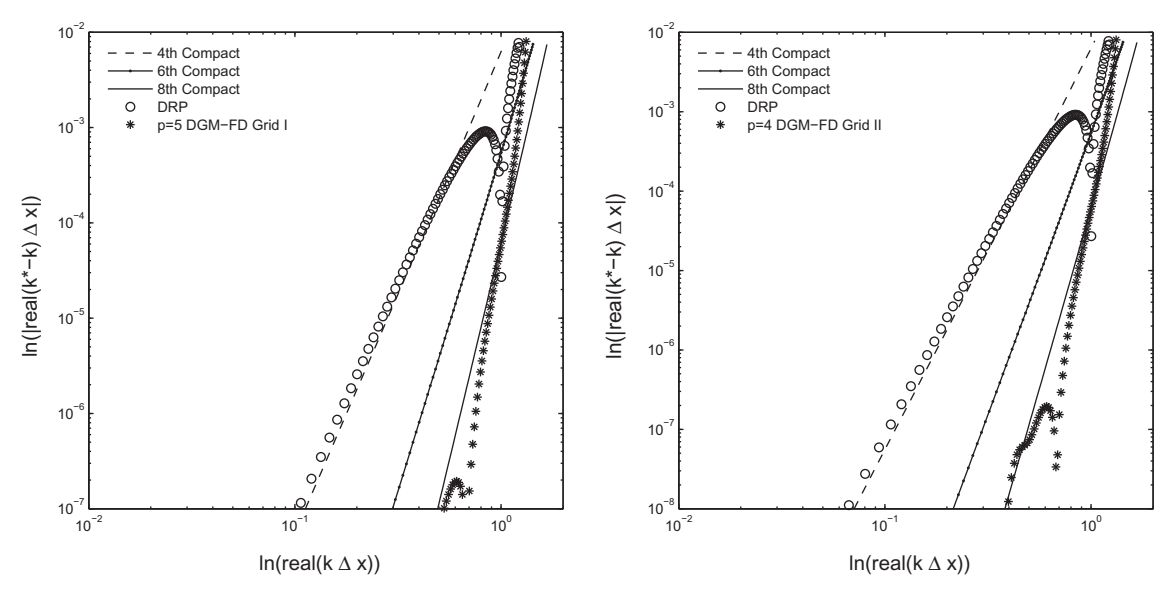


Fig. 14. log log(Real(k*-k)) compact, DRP, DGM-FD. Left: Grid I and right: Grid II.

7. Numerical examples

In this section, we show numerical examples of the scheme presented in this paper. As the applications are two dimensional, the spatial derivatives are performed with DGM-FD in each dimension. In all the examples, method of lines is employed with five stage Runge–Kutta as the time integration scheme [21].

7.1. Linear waves in free space

We solve the linearized Euler equations rewritten as:

$$\frac{\partial \mathbf{U}}{\partial t} + \mathbf{A} \frac{\partial \mathbf{U}}{\partial x} + \mathbf{B} \frac{\partial \mathbf{U}}{\partial y} = 0 \tag{39}$$

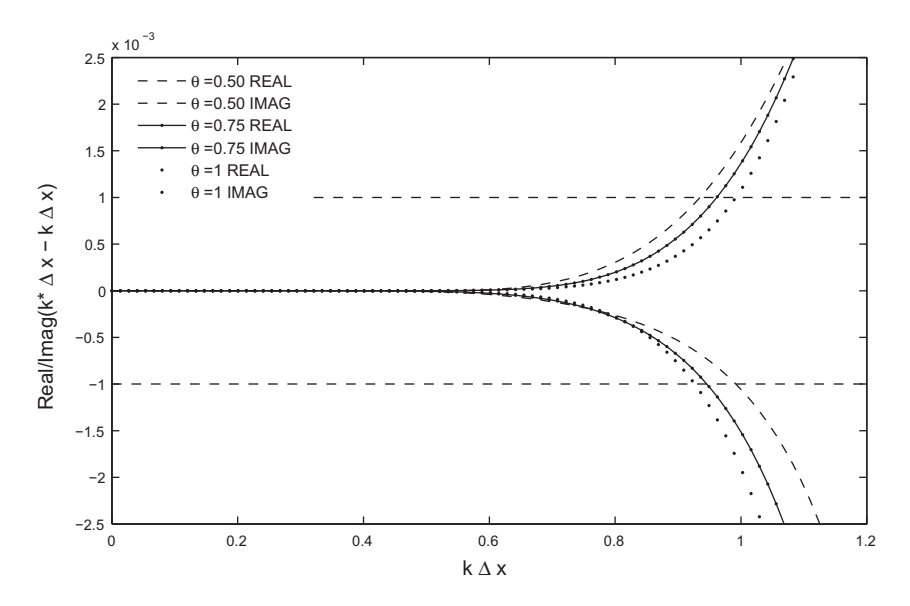


Fig. 15. Real $(k^* - k)$ and Imag $(k^* - k)$ θ = 0.50, 0.75, 1.

where **A** and **B** are the coefficient matrices:

$$\mathbf{A} = \begin{bmatrix} M_x & 1 & 0 & 0 \\ 0 & M_x & 0 & 1 \\ 0 & 0 & M_x & 0 \\ 0 & 1 & 0 & M_x \end{bmatrix}, \quad \mathbf{B} = \begin{bmatrix} M_y & 0 & 1 & 0 \\ 0 & M_y & 0 & 0 \\ 0 & 0 & M_y & 1 \\ 0 & 0 & 1 & M_y \end{bmatrix}, \quad \mathbf{U} = \begin{bmatrix} \rho \\ u \\ v \\ p \end{bmatrix}$$

In the above, ρ is density, u and v are velocities in x and y directions, respectively, p is pressure and M_x and M_y are constant mean flow Mach numbers in the x and y directions, respectively. The computational domain is $[-110,110] \times [-110,110]$ with the Perfectly Matched Layer absorbing condition applied for the 10 grid points around the boundary [23]. For the example, $M_x = 0.5$, $M_y = 0$. Grid I scheme of p = 5 given in Section 3 is applied in this example.

For this linear problem **A**, **B** can be decomposed into sums of matrices with positive and negative eigenvalues. In this way, we rewrite (39) as:

$$\frac{\partial \mathbf{U}}{\partial t} = -\left[(\mathbf{A}^+ + \mathbf{A}^-) \frac{\partial \mathbf{U}}{\partial x} + (\mathbf{B}^+ + \mathbf{B}^-) \frac{\partial \mathbf{U}}{\partial y} \right]$$

or

$$\frac{\partial \mathbf{U}}{\partial t} = -[(\mathbf{A}^{+}\mathbf{D}_{x}^{+} + \mathbf{A}^{-}\mathbf{D}_{x}^{-})\mathbf{U} + (\mathbf{B}^{+}\mathbf{D}_{y}^{+} + \mathbf{B}^{-}\mathbf{D}_{y}^{-})\mathbf{U}]$$

where:

$$\boldsymbol{A}^{+} = \begin{bmatrix} M_{x} & (M_{x}+1)/2 & 0 & (1-M_{x})/2 \\ 0 & (M_{x}+1)/2 & 0 & (M_{x}+1)/2 \\ 0 & 0 & M_{x} & 0 \\ 0 & (M_{x}+1)/2 & 0 & (M_{x}+1)/2 \end{bmatrix}, \quad \boldsymbol{A}^{-} = \begin{bmatrix} 0 & -(M_{x}-1)/2 & 0 & (M_{x}-1)/2 \\ 0 & (M_{x}-1)/2 & 0 & -(M_{x}-1)/2 \\ 0 & 0 & 0 & 0 \\ 0 & -(M_{x}-1)/2 & 0 & (M_{x}-1)/2 \end{bmatrix}$$

$$\boldsymbol{B}^{+} = \begin{bmatrix} M_y & 0 & (M_y+1)/2 & (1-M_y)/2 \\ 0 & M_y & 0 & 0 \\ 0 & 0 & (M_y+1)/2 & (M_y+1)/2 \\ 0 & 0 & (M_y+1)/2 & (M_y+1)/2 \end{bmatrix}, \quad \boldsymbol{B}^{-} = \begin{bmatrix} 0 & 0 & -(M_y-1)/2 & (M_y-1)/2 \\ 0 & 0 & 0 & 0 \\ 0 & 0 & (M_y-1)/2 & -(M_y-1)/2 \\ 0 & 0 & -(M_y-1)/2 & (M_y-1)/2 \end{bmatrix}$$

The derivative formula in terms of the solution variable u, (17), is used where a = 1 for \mathbf{D}_{x}^{+} , \mathbf{D}_{y}^{+} and a = -1 for \mathbf{D}_{x}^{-} , \mathbf{D}_{y}^{-} operators, respectively.

Fig. 16 shows the computational domain with variable grid spacings. For grids in x direction, grid spacing starts with $\Delta x_1 = 1$ (with element width $h = p\Delta x_1 = 5$). Two sub-regions with $\Delta x_2 = \frac{1}{5}$, and $h = p\Delta x_2 = 1$ are introduced as shown. The grids

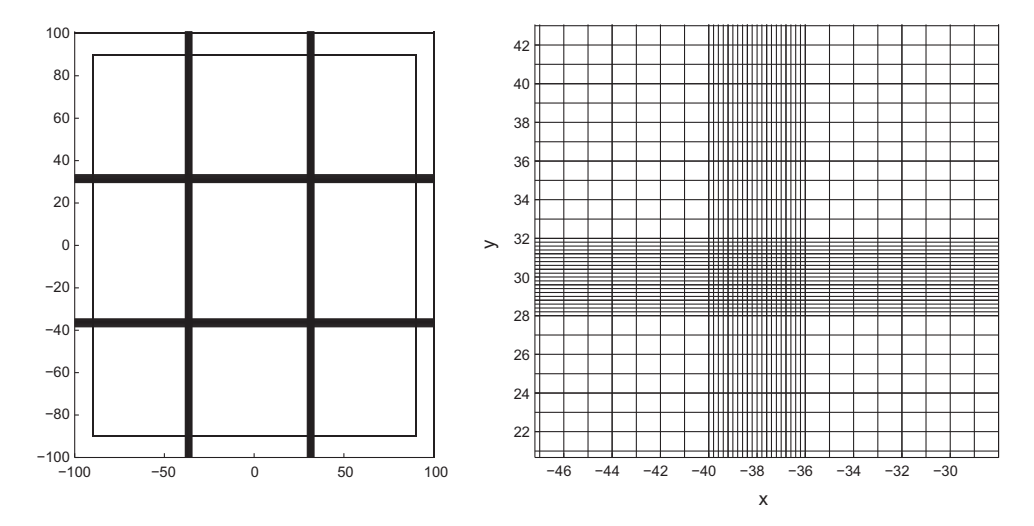


Fig. 16. Computational domain with variable grid sizes.

in the *y*-direction are similarly structured. The total number of collocation points on each direction is 315. The initial condition is the following:

$$\begin{split} &\rho(x,y,0) = e^{\left[-\ln(2)\left(\frac{x^2+y^2}{9}\right)\right]} + 0.1e^{\left[-\ln(2)\left(\frac{(x-67)^2+y^2}{25}\right)\right]}, \quad u(x,y,0) = 0.04ye^{\left[-\ln(2)\left(\frac{(x-67)^2+y^2}{25}\right)\right]} \\ &\nu(x,y,0) = -0.04(x-67)e^{\left[-\ln(2)\left(\frac{(x-67)^2+y^2}{25}\right)\right]}, \quad p(x,y,0) = e^{\left[-\ln(2)\left(\frac{x^2+y^2}{9}\right)\right]} \end{split}$$

This is a Benchmark problem in Computational Aeroacousitics (CAA). It includes an acoustic pulse, vorticity wave and entropy wave. Density contours and a comparison with the exact solution are shown in Figs. 17 and 18. The numerical solution appears to be smooth at grid interfaces and agrees very well with the exact solutions.

7.2. Acoustic pulse reflection by a wall

In this example, an acoustic pulse is the reflected by a solid wall. The computational domain is $[-110,110] \times [0,220]$. A solid wall is located at y = 0. The PML absorbing condition is applied for the 10 grid points on the left and right and 20 grid points on the top boundary of the computational domain [23]. The fourth order Grid II scheme, given in Section 4, will be applied in this example with following initial condition:

$$p(x,y,0) = \rho(x,y,0) = e^{[-\ln(2)(\frac{x^2+(y-25)^2}{25})]}, \quad u(x,y,0) = v(x,y,0) \equiv 0$$

Density contours are shown in Fig. 19. A good comparison with the exact solution is found.

7.3. Burger's equation

To demonstrate the ability of the scheme for treating higher order derivatives, we show an example of the Burger's equation. The governing equation is:

$$\frac{\partial u}{\partial t} + \frac{1}{2} \frac{\partial (u^2)}{\partial x} = v \frac{\partial^2 u}{\partial x^2}$$

where v is taken to be 0.02.

The equation admits an exact solution:

$$u(x,t)=1-tanh\bigg(\frac{x-x_c-t}{2v}\bigg),\quad x_c=5$$

where x_c is the location of the wave front at t = 0. The boundary and initial conditions are given below. As the wave front changes rapidly over a small region in the domain, the grid size changes from Δx = 0.2 in the coarse part of the grid to Δx = 0.025 in the refined region [30]. The initial and boundary conditions are:

$$\begin{split} & \textit{IC}: \quad \textit{u}(\textit{x},0) = 1 - \textit{tanh}\Big(\frac{\textit{x} - \textit{x}_c}{2\nu}\Big), \quad \textit{x}_c = 5 \\ & \textit{BC}: \quad \textit{u}(0,t) = 2, \quad \textit{u}(\infty,t) = 0 \end{split}$$

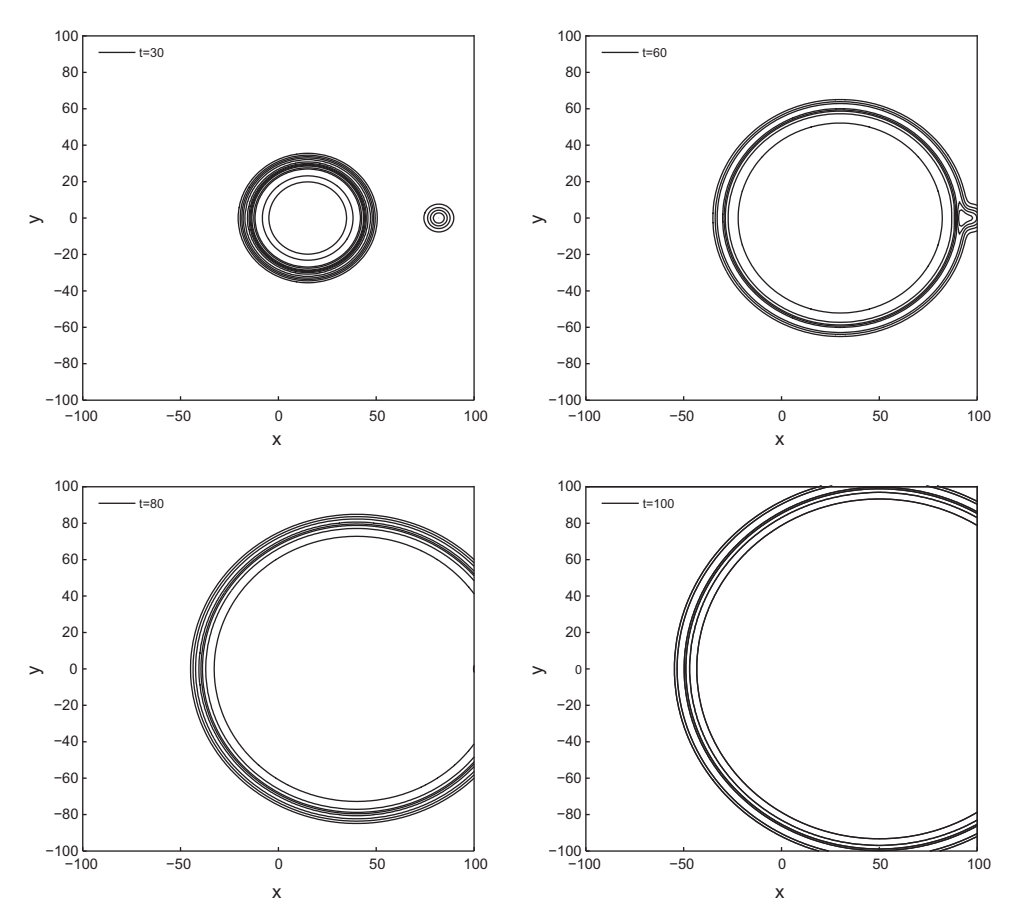


Fig. 17. Contours of density at t = 30, 60, 80, 100 in the physical domain using Grid Structure I, p = 5.

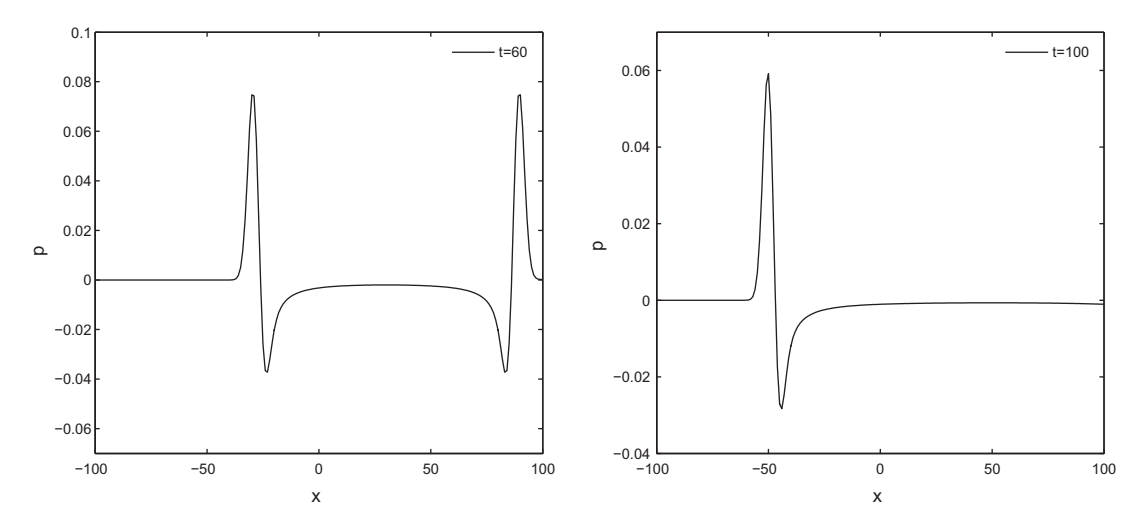


Fig. 18. Comparison of pressure with exact solution along y = 0 using Grid Structure I, p = 5.

Grid II, as given in Section 4, is used. The flux, $f = \frac{1}{2}u^2$ and the value of λ in the difference formula (27) is taken to be 1. The second derivative for u was evaluated using (D+)(D-) where D± is the difference formula given in (28) with corresponding + and - sign, respectively.

Time integration is again the five stage Runge–Kutta [21] where Δt is conservatively chosen to be 0.025 times the smallest Δx , 0.02 or Δt = 0.000625.

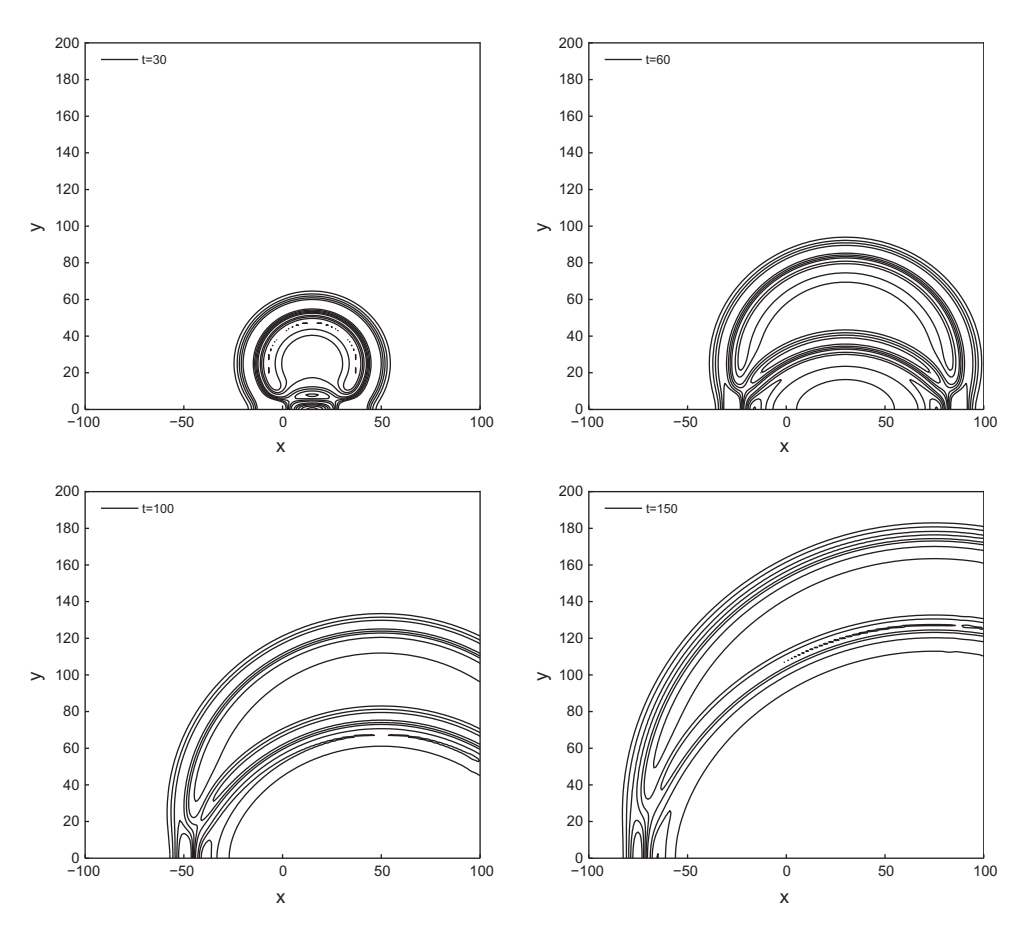


Fig. 19. Contours of density at t = 30, 60, 100, 150 in the physical domain using Grid Structure II, p = 4.

Fig. 20 shows the numerical and exact solution at t = 30 as well as the computational domain with a variable grid that is more refined in the area supporting the wave front. One such grid is shown below. Note the close up of the numerical solution and the good agreement between the numerical and exact solutions.

The computational domain is initially [0,40]. In order to verify the accuracy and stability over a longer time period, with a final time of 420, a moving grid frame is used. For the adaptive grid, the code checks to see if the wave front is moving too far away from the center of the refined region and then, if so, refines a unit on the right of the region while coarsening a unit on the left. As the wave front is still well within the refined region this results in refining an area of the solution that is constant, through interpolation, and coarsening an area that is also constant through interpolation. In this way the adaptive grid is dynamic.

The shape of the numerical solution remains nearly constant for time from 0 to 420 and the numerical solution is stable as shown in Fig. 21. Again we note the strong agreement between numerical and exact solutions.

7.4. Flat-plate boundary layer problem

In this example, we apply the DGM-FD scheme shown in (16) to the computation of a steady-state boundary layer profile formed by a uniform flow over a flat plate. The governing equations are the Navier–Stokes equations [25]

$$\frac{\partial \mathbf{U}}{\partial t} + \frac{\partial \mathbf{E}}{\partial x} + \frac{\partial \mathbf{F}}{\partial y} = 0 \tag{40}$$

where

$$\mathbf{U} = \begin{bmatrix} \rho \\ \rho u \\ \rho v \\ \rho e \end{bmatrix}$$

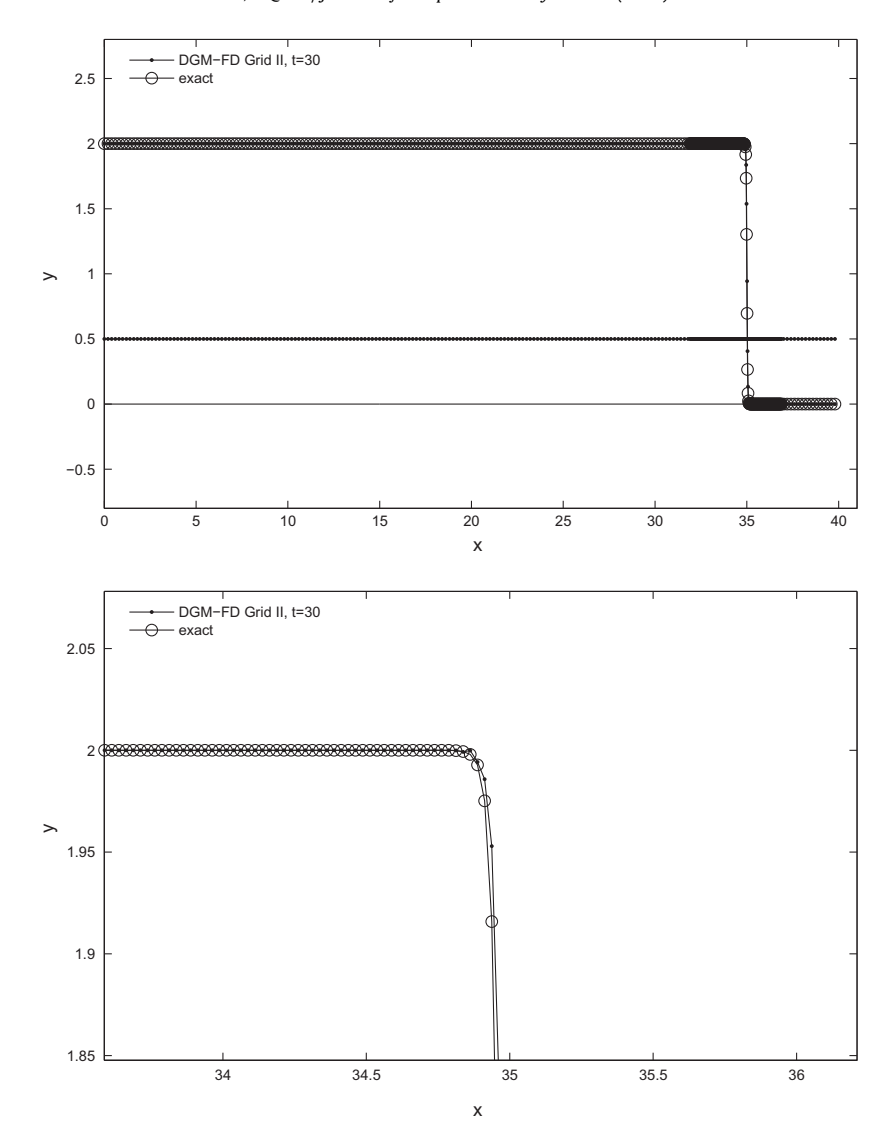


Fig. 20. Burger's equation, DGM-FD Grid II, p = 4, 8:1 refinement, log of error = -2.4470; top: plot of exact and numerical solution at t = 30 and bottom: zoom at t = 30 of exact and numerical solution.

and flux vectors

$$\mathbf{E} = \begin{bmatrix} \rho u \\ \rho u^2 + p - \tau_{xx} \\ \rho u v - \tau_{xy} \\ (\rho e + p) u - u \tau_{xx} - v \tau_{xy} + q_x \end{bmatrix}$$

$$\mathbf{F} = \begin{bmatrix} \rho v \\ \rho u v - \tau_{xy} \\ \rho v^2 + p - \tau_{yy} \\ (\rho e + p) v - u \tau_{xy} - v \tau_{yy} + q_y \end{bmatrix}$$

with viscous stress terms written as

$$\begin{split} &\tau_{xx} = \frac{M_x}{Re_N} \left[2\mu \frac{\partial u}{\partial x} - \lambda (\frac{\partial u}{\partial x} + \frac{\partial \nu}{\partial y}) \right], \quad \tau_{yy} = \frac{M_x}{Re_N} \left[2\mu \frac{\partial \nu}{\partial y} - \lambda \left(\frac{\partial u}{\partial x} + \frac{\partial \nu}{\partial y} \right) \right] \\ &\lambda = \frac{2}{3}\mu, \quad \tau_{xy} = \frac{M_x}{Re_N} \mu \left(\frac{\partial u}{\partial y} + \frac{\partial \nu}{\partial x} \right) \end{split}$$

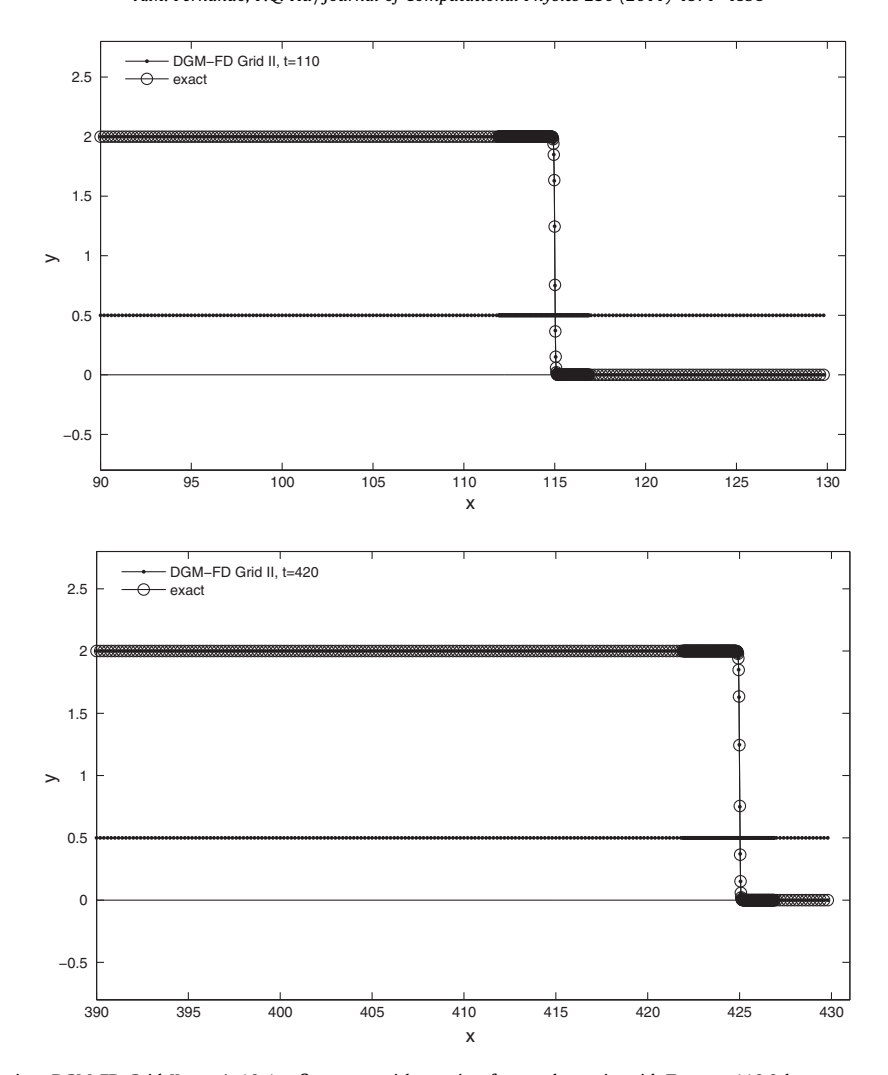


Fig. 21. Burger's equation, DGM-FD Grid II, p = 4, 10:1 refinement with moving frame, dynamic grid. Top: t = 110.0 log norm error = -2.3929; Bottom: ts = 420.0 log norm error = -2.3929.

and heat transfer terms

$$q_x = -\frac{M_x}{(\gamma-1)PrRe_N}\mu\frac{\partial T}{\partial x}, \quad q_y = -\frac{M_x}{(\gamma-1)PrRe_N}\mu\frac{\partial T}{\partial y}$$

where viscosity, μ , non-dimensionalized by a reference value, μ_{∞} , is assumed to be unity. The equation of state and the energy function are

$$\gamma p = \rho T, \quad e = \frac{u^2 + \nu^2}{2} + \frac{p}{(\gamma - 1)\rho}$$

In the above, u and v are the velocity components in the x and y directions, respectively, p is the pressure, ρ the density, and T is the temperature, the Prandtl number, Pr is 0.708 and γ the specific heats ratio. The velocity is non-dimensionalized by a reference speed of sound, a_{∞} , density by ρ_{∞} and pressure by $\rho_{\infty}a_{\infty}^2$. The Reynolds number, Re_N , is $\rho_{\infty}U_{\infty}L_{\infty}/\mu_{\infty}$ where U_{∞} is a characteristic flow velocity and L_{∞} , a length scale. As ${\bf E}$ and ${\bf F}$ are composed of the primitive variables, ρ , u, v, and p, the derivatives of each are computed using (16). In this way expressions τ_{xx} , τ_{xy} and τ_{yy} , which are made up of derivatives of the primitives with respect to x or y, are evaluated. The spatial derivatives in (40) are computed using (16) with θ = 0.5 and Grid II coefficients are applied. The magnitude of the largest eigenvalue over the domain of ${\bf U}$ of the Jacobians of ${\bf E}$, ${\bf F}$ is taken to be λ = 1.1 and included in (40).

This application is shown with Reynolds number of 5000. A schematic of the domain is shown in Fig. 22. The incoming flow is uniform in the direction of the *x*-axis with Mach number, $M = U_{\infty}/a_{\infty} = 0.1$. Numerical calculation starts with an initialization of all variables in the physical domain by the uniform incoming flow:

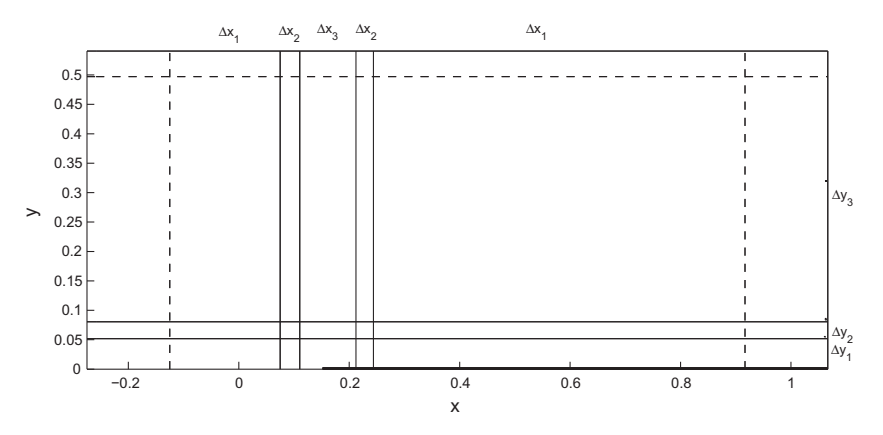


Fig. 22. Top: Schematic of domain. In particular are grid lines where dx and dy change and boundary condition locations, $Re_N = 5000$ with dashed lines for PML boundaries with grid, left to right, is dx = 0.0083, 0.0042, 0.0007, 0.0042, 0.0083 and, bottom to top, dy = 0.0006, 0.0012, 0.0024.

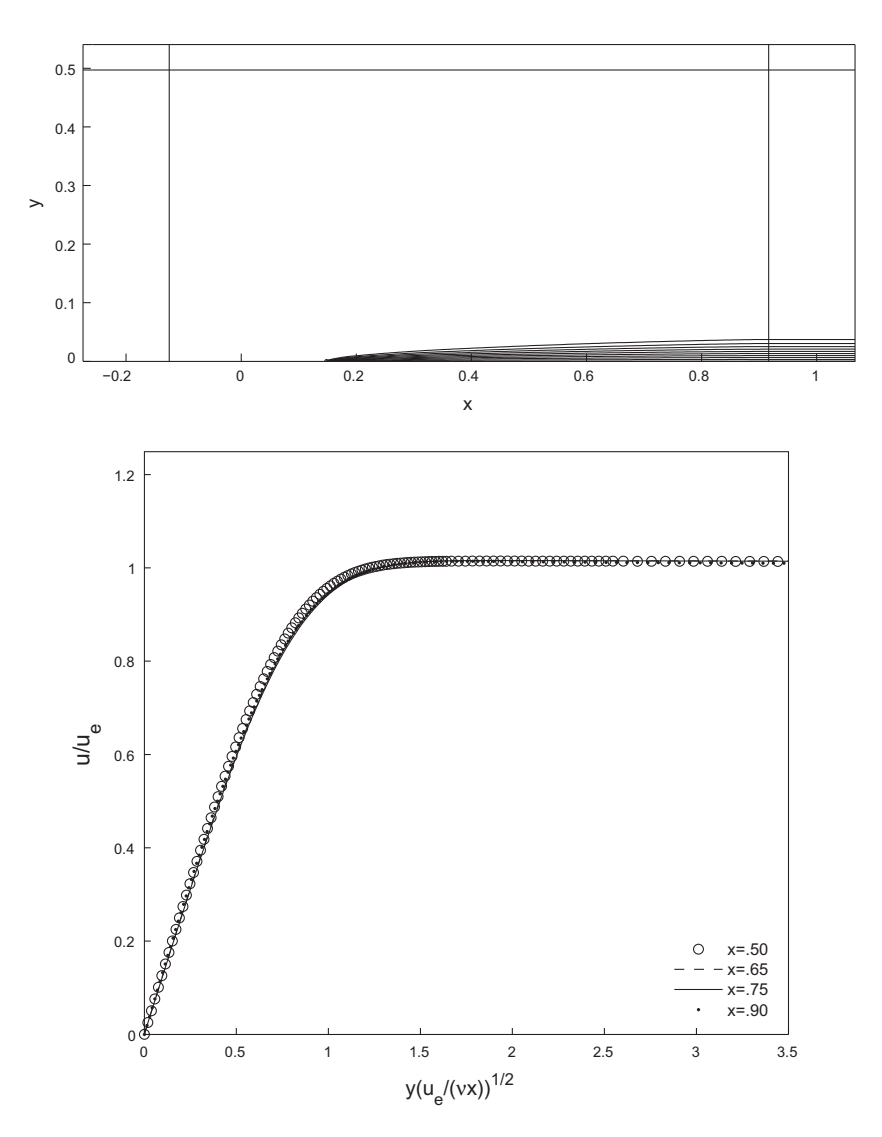


Fig. 23. Top: Boundary layer of stream-wise velocity $Re_N = 5000$ at t = 20.00 including borders of PML region; Bottom: Similarity velocity profile at x = 0.50, 0.65, 0.75, 0.90. Horizontal variable is $y (u_e/(vx))^{1/2}$ and u_e is the exterior stream-wise velocity, 0.1.

$$\rho(x,y,0) = 1, \quad u(x,y,0) = u_e = 0.1, \quad \nu(x,y,0) = 0.0, \quad p(x,y,0) = \frac{1}{\gamma}, \quad \gamma = 1.4$$

The variable grid structure has three distinct regions with respect to the *y*-axis as greater refinement is needed on the region closest to the plate (see Fig. 22). For the *y*-axis the refined region starts with a 4:1 ratio then transitions to a 2:1 ratio and finally to the non-refined portion. Likewise, with respect to the *x*-axis a 2:1, 12:1 then 2:1 refinement is shown and there are five regions here where the third region, 12:1, includes the plate leading edge where extra refinements are necessary because of the high Reynolds number. PML boundary conditions of [25] are used at the three boundaries where the pseudo mean flow is adjusted after each Runge–Kutta time loop. Dashed lines in Fig. 22 indicate the PML interfaces.

Fig. 23, top, shows the contours of the u-velocity in the whole computational domain with borders of PML region and Fig. 23, bottom, shows the normalized stream-wise velocity profile where the stream-wise velocity is plotted as a function of a similarity variable, $y\sqrt{u_e/(vx)}$, with $\frac{u_e}{v}=5000$, at x=0.50, 0.65, 0.75, and 0.90. The similarity solutions, again, show good agreement.

8. Conclusions

Numerical schemes for computational aeroacoustics problems require low dissipation and low dispersion errors along with high order accuracy, flexibility with variable grid refinements, and then preferably, ease of use. There are many methods that do some of these things well, at the expense of others. The method introduced in this research, DGM-FD, is an attempt to formulate a spatial derivative scheme as one that achieves some of requirements of effective numerical schemes for CAA. DGM-FD is a finite difference type method that has high-order convergence with strong accuracy for numerical wave numbers and is adaptive to non-uniform grids. Inherited from DGM, the proposed scheme retains super-accuracy for wave propagations. Of the two grid structures presented, the Grid Structure I has a shortened stencil for the derivative scheme, with some grid points being double-valued. The Grid Structure II uses directly a finite difference type grid and is, again, adaptive for non-uniform grid spacings regions. For non-linear applications the general flux finite difference formula (16) is presented where no explicit upwind and downwind split of the flux is required. The schemes achieve stable boundary closures while retaining the formal and wave number super-accuracy for wave propagation problems. Good results in the numerical examples demonstrate the effectiveness of the new schemes.

Acknowledgments

This work is supported in part by a grant from the National Science Foundation DMS-0810946 and the Old Dominion University Graduate Fellowship.

Appendix A. Third order coefficients for Grid Structure I

Third and fourth order (p = 3,4) scheme for interior points are presented. Recall that h_n is the element length and that for interior elements, $h_n = p\Delta x$. To be used for (22) and (24).

Third order coefficients with second order closure:

$$\mathbf{D} = \begin{bmatrix} -4 & \frac{5}{4} & \frac{9}{2} & -\frac{9}{4} & \frac{3}{2} & -1\\ \frac{17}{27} & -\frac{61}{54} & -\frac{3}{4} & \frac{3}{2} & -\frac{59}{108} & \frac{8}{27}\\ -\frac{8}{27} & \frac{59}{108} & -\frac{3}{2} & \frac{3}{4} & \frac{61}{54} & -\frac{17}{27}\\ 1 & -\frac{3}{2} & \frac{9}{4} & -\frac{9}{2} & -\frac{5}{4} & 4 \end{bmatrix} \quad \text{and} \quad \mathbf{D}' = \begin{bmatrix} -4 & 4 & 0 & 0 & -1 & 1\\ \frac{17}{27} & -\frac{17}{27} & 0 & 0 & \frac{8}{27} & -\frac{8}{27}\\ -\frac{8}{27} & \frac{8}{27} & 0 & 0 & -\frac{17}{27} & \frac{17}{27}\\ 1 & -1 & 0 & 0 & 4 & -4 \end{bmatrix}$$

$$\mathbf{D}^{cl} = \begin{bmatrix} -\frac{3}{2} & 2 & -\frac{5}{4} & \frac{3}{4}\\ -\frac{1}{2} & 0 & \frac{7}{8} & -\frac{3}{8}\\ \frac{1}{2} & -2 & -\frac{3}{4} & \frac{9}{4} \end{bmatrix} \quad \text{and} \quad \mathbf{D}'^{cl} = \begin{bmatrix} 0 & 0 & \frac{3}{4} & -\frac{3}{4}\\ 0 & 0 & -\frac{3}{8} & \frac{3}{8}\\ 0 & 0 & \frac{9}{4} & -\frac{9}{4} \end{bmatrix}$$

Appendix B. Fourth order coefficients for Grid Structure I

Fourth order coefficients with third order closure:

$$\mathbf{D} = \begin{bmatrix} -\frac{25}{4} & \frac{25}{12} & 8 & -6 & \frac{8}{3} & -\frac{7}{4} & \frac{5}{4} \\ \frac{485}{512} & -\frac{741}{512} & -\frac{5}{3} & 3 & -1 & \frac{511}{1536} & -\frac{85}{512} \\ -\frac{15}{32} & \frac{69}{61} & -\frac{4}{3} & 0 & \frac{4}{3} & -\frac{61}{96} & \frac{15}{32} \\ \frac{85}{512} & -\frac{511}{1536} & 1 & -3 & \frac{5}{3} & \frac{741}{512} & -\frac{485}{512} \\ -\frac{5}{4} & \frac{7}{4} & -\frac{8}{3} & 6 & -8 & -\frac{25}{12} & \frac{25}{4} \end{bmatrix} \end{bmatrix} \text{ and } \mathbf{D}' = \begin{bmatrix} -\frac{25}{4} & \frac{25}{4} & 0 & 0 & 0 & \frac{5}{4} & -\frac{5}{4} \\ \frac{485}{512} & -\frac{485}{512} & 0 & 0 & 0 & -\frac{85}{512} & \frac{85}{512} \\ -\frac{15}{32} & \frac{15}{32} & 0 & 0 & 0 & \frac{15}{32} & -\frac{15}{32} \\ \frac{85}{512} & -\frac{512}{512} & 0 & 0 & 0 & -\frac{485}{512} & \frac{485}{512} \\ -\frac{5}{4} & \frac{7}{4} & -\frac{8}{3} & 6 & -8 & -\frac{25}{12} & \frac{25}{4} \end{bmatrix}$$

$$\mathbf{D}^{cl} = \begin{bmatrix} -\frac{11}{4} & \frac{9}{2} & -\frac{9}{4} & \frac{3}{2} & -1\\ -\frac{1}{2} & -\frac{3}{4} & \frac{3}{2} & -\frac{59}{108} & \frac{8}{27}\\ \frac{1}{4} & -\frac{3}{2} & \frac{3}{4} & \frac{61}{54} & -\frac{17}{27}\\ -\frac{1}{2} & \frac{9}{4} & -\frac{9}{2} & -\frac{5}{4} & 4 \end{bmatrix} \text{ and } \mathbf{D}^{v,cl} = \begin{bmatrix} 0 & 0 & 0 & -1 & 1\\ 0 & 0 & 0 & \frac{8}{27} & -\frac{8}{27}\\ 0 & 0 & 0 & -\frac{17}{27} & \frac{17}{27}\\ 0 & 0 & 0 & 4 & -4 \end{bmatrix}$$

Appendix C. Second order coefficients for Grid Structure II

The second and third order (p = 2,3) scheme for interior points is presented. Recall that h_n is the element length and that for interior elements, $h_n = (p + 1)\Delta x$.

Then by (16), the finite difference formula for a set of three grid points, second order, is given by

$$\frac{\partial}{\partial x} \begin{bmatrix} f_{n0} \\ f_{n1} \\ f_{n2} \end{bmatrix} = \frac{2}{\mathbf{h}_{n}} \overline{\mathbf{M}}_{-} \begin{bmatrix} f_{(n-1)0} \\ f_{(n-1)1} \\ f_{(n-1)2} \end{bmatrix} + \frac{2}{\mathbf{h}_{n}} \overline{\mathbf{M}}_{0} \begin{bmatrix} f_{n0} \\ f_{n1} \\ f_{n2} \end{bmatrix} + \frac{2}{\mathbf{h}_{n}} \overline{\mathbf{M}}_{+} \begin{bmatrix} f_{(n+1)0} \\ f_{(n+1)1} \\ f_{(n+1)2} \end{bmatrix} + \frac{2}{\mathbf{h}_{n}} \theta \lambda \overline{\mathbf{M}}_{-} \begin{bmatrix} u_{(n-1)0} \\ u_{(n-1)1} \\ u_{(n-1)2} \end{bmatrix} + \frac{2}{\mathbf{h}_{n}} \theta \lambda \overline{\mathbf{N}}_{0} \begin{bmatrix} u_{n0} \\ u_{n1} \\ u_{n2} \end{bmatrix} - \frac{2}{\mathbf{h}_{n}} \theta \lambda \overline{\mathbf{M}}_{+} \begin{bmatrix} u_{(n+1)0} \\ u_{(n+1)1} \\ u_{(n+1)2} \end{bmatrix}$$
(C.1)

where using (25) and (20), it is found that

$$\overline{\mathbf{M}}_{-} = \begin{bmatrix} -\frac{23}{64} & \frac{115}{96} & -\frac{115}{64} \\ \frac{9}{64} & -\frac{15}{32} & \frac{45}{64} \\ \frac{1}{64} & -\frac{5}{96} & \frac{5}{64} \end{bmatrix}, \quad \overline{\mathbf{M}}_{\mathbf{0}} = \begin{bmatrix} -\frac{7}{16} & \frac{7}{4} & -\frac{5}{16} \\ -\frac{21}{16} & \mathbf{0} & \frac{21}{16} \\ \frac{5}{16} & -\frac{7}{4} & \frac{7}{16} \end{bmatrix}$$

$$\overline{\mathbf{N_0}} = \begin{bmatrix} \frac{57}{32} & -\frac{55}{48} & \frac{9}{32} \\ -\frac{27}{32} & \frac{15}{16} & -\frac{27}{32} \\ \frac{9}{32} & -\frac{55}{48} & \frac{57}{32} \end{bmatrix}, \quad \overline{\mathbf{M}}_+ = \begin{bmatrix} -\frac{5}{64} & \frac{5}{96} & -\frac{1}{64} \\ -\frac{45}{64} & \frac{15}{32} & -\frac{9}{64} \\ \frac{165}{64} & -\frac{115}{96} & \frac{23}{64} \end{bmatrix}$$

For the first element:

$$\frac{\partial}{\partial x} \begin{bmatrix} f_{00} \\ f_{01} \end{bmatrix} = \frac{2}{h_0} \left(\overline{\mathbf{M}}_{\mathbf{10}}^{\alpha} + \overline{\mathbf{M}}_{\mathbf{20}}^{\alpha} \right) \begin{bmatrix} f_{00} \\ f_{01} \end{bmatrix} + \frac{2}{\mathbf{h_0}} \overline{\mathbf{M}}_{+}^{\alpha} \begin{bmatrix} f_{10} \\ f_{11} \\ f_{12} \end{bmatrix} + \frac{2}{\mathbf{h_0}} \theta \lambda \left(\overline{\mathbf{M}}_{\mathbf{10}}^{\alpha} + \overline{\mathbf{M}}_{\mathbf{20}}^{\alpha} \right) \begin{bmatrix} u_{00} \\ u_{01} \end{bmatrix} - \frac{2}{\mathbf{h_0}} \theta \lambda \overline{\mathbf{M}}_{+}^{\alpha} \begin{bmatrix} u_{10} \\ u_{11} \\ u_{12} \end{bmatrix}$$
(C.2)

$$\overline{\boldsymbol{M}}_{\boldsymbol{10}}^{\alpha} = \begin{bmatrix} -1 & 0 \\ 0 & 0 \end{bmatrix}, \quad \overline{\boldsymbol{M}}_{\boldsymbol{20}}^{\alpha} = \begin{bmatrix} 0 & \frac{3}{2} \\ -\frac{1}{2} & 0 \end{bmatrix}$$

$$\overline{\bm{N}}_0^\alpha = \begin{bmatrix} \frac{5}{4} & -\frac{3}{4} \\ -\frac{1}{4} & \frac{3}{4} \end{bmatrix}, \quad \overline{\bm{M}}_+^\alpha = \begin{bmatrix} -\frac{15}{16} & \frac{5}{8} & -\frac{3}{16} \\ \frac{15}{16} & -\frac{5}{8} & \frac{3}{16} \end{bmatrix}$$

For the second element, the 2nd order flux scheme:

$$\frac{\partial}{\partial x} \begin{bmatrix} f_{10} \\ f_{11} \\ f_{12} \end{bmatrix} = \frac{2}{h_1} \overline{\mathbf{M}}_{-}^{\beta} \begin{bmatrix} f_{00} \\ f_{01} \end{bmatrix} + \frac{2}{\mathbf{h_1}} \overline{\mathbf{M}}_{\mathbf{0}}^{\beta} \begin{bmatrix} f_{10} \\ f_{11} \\ f_{12} \end{bmatrix} + \frac{2}{\mathbf{h_1}} \overline{\mathbf{M}}_{+}^{\beta} \begin{bmatrix} f_{20} \\ f_{21} \\ f_{22} \end{bmatrix} + \frac{2}{\mathbf{h_1}} \theta \lambda \overline{\mathbf{M}}_{-}^{\beta} \begin{bmatrix} u_{00} \\ u_{01} \end{bmatrix} + \frac{2}{\mathbf{h_1}} \theta \lambda \overline{\mathbf{N}}_{\mathbf{0}}^{\beta} \begin{bmatrix} u_{10} \\ u_{11} \\ u_{12} \end{bmatrix} - \frac{2}{\mathbf{h_1}} \theta \lambda \overline{\mathbf{M}}_{+}^{\beta} \begin{bmatrix} u_{20} \\ u_{21} \\ u_{22} \end{bmatrix}$$
(C.3)

$$\overline{\mathbf{M}}_{-}^{\beta} = \begin{bmatrix} \frac{23}{48} & -\frac{23}{16} \\ -\frac{3}{16} & \frac{9}{16} \\ -\frac{1}{48} & \frac{1}{16} \end{bmatrix}, \quad \overline{\mathbf{M}}_{\mathbf{0}}^{\beta} = \begin{bmatrix} -\frac{7}{16} & \frac{7}{4} & -\frac{5}{16} \\ -\frac{21}{16} & 0 & \frac{21}{16} \\ \frac{5}{16} & -\frac{7}{4} & \frac{7}{16} \end{bmatrix}$$

$$\overline{\mathbf{N_0^{\beta}}} = \begin{bmatrix} \frac{57}{32} & -\frac{55}{48} & \frac{9}{32} \\ -\frac{27}{32} & \frac{15}{16} & -\frac{27}{32} \\ \frac{9}{32} & -\frac{55}{48} & \frac{57}{32} \end{bmatrix}, \quad \overline{\mathbf{M}}_{+}^{\beta} = \begin{bmatrix} -\frac{5}{64} & \frac{5}{96} & -\frac{1}{64} \\ -\frac{45}{64} & \frac{15}{32} & -\frac{9}{64} \\ \frac{115}{64} & -\frac{115}{96} & \frac{23}{64} \end{bmatrix}$$

Appendix D. Third order coefficients for Grid Structure II

For the third order scheme, again by (16), the finite difference formula for a set of four grid points is given by

$$\frac{\partial}{\partial x} \begin{bmatrix} f_{n0} \\ f_{n1} \\ f_{n2} \\ f_{n3} \end{bmatrix} = \frac{2}{\mathbf{h}_n} \overline{\mathbf{M}}_- \begin{bmatrix} f_{(n-1)0} \\ f_{(n-1)1} \\ f_{(n-1)2} \\ f_{(n-1)3} \end{bmatrix} + \frac{2}{\mathbf{h}_n} \overline{\mathbf{M}}_0 \begin{bmatrix} f_{n0} \\ f_{n1} \\ f_{n2} \\ f_{n3} \end{bmatrix} + \frac{2}{\mathbf{h}_n} \overline{\mathbf{M}}_+ \begin{bmatrix} f_{(n+1)0} \\ f_{(n+1)1} \\ f_{(n+1)2} \\ f_{(n+1)3} \end{bmatrix} + \frac{2}{\mathbf{h}_n} \theta \lambda \overline{\mathbf{M}}_- \begin{bmatrix} u_{(n-1)0} \\ u_{(n-1)1} \\ u_{(n-1)2} \\ u_{(n-1)3} \end{bmatrix} + \frac{2}{\mathbf{h}_n} \theta \lambda \overline{\mathbf{N}}_0 \begin{bmatrix} u_{n0} \\ u_{n1} \\ u_{n2} \\ u_{n3} \end{bmatrix} - \frac{2}{\mathbf{h}_n} \theta \lambda \overline{\mathbf{M}}_+ \begin{bmatrix} u_{(n+1)0} \\ u_{(n+1)1} \\ u_{(n+1)2} \\ u_{(n+1)3} \end{bmatrix}$$
(D.1)

where using (25) and (20), it is found that

$$\overline{\mathbf{M}}_{-} = \begin{bmatrix} \frac{2865}{8192} & -\frac{12033}{8192} & \frac{20055}{8192} & -\frac{20055}{8192} \\ -\frac{1685}{8192} & \frac{7077}{8192} & -\frac{11795}{8192} & \frac{11795}{8192} \\ \frac{365}{8192} & -\frac{1533}{8192} & \frac{2555}{8192} & -\frac{2553}{8192} \\ \frac{615}{8192} & -\frac{2583}{8192} & \frac{4305}{8192} & -\frac{4305}{8192} \end{bmatrix}, \quad \overline{\mathbf{M}}_{\mathbf{0}} = \begin{bmatrix} -\frac{14051}{12288} & \frac{13257}{4096} & -\frac{4119}{4096} & -\frac{2563}{12288} \\ -\frac{25337}{12288} & \frac{4096}{4096} & \frac{4096}{4096} & -\frac{2563}{12288} \\ -\frac{5401}{12288} & \frac{5401}{4096} & \frac{5931}{4096} & \frac{25337}{12288} \\ \frac{2563}{12288} & \frac{4119}{4096} & -\frac{13257}{4096} & \frac{14051}{12288} \end{bmatrix}$$

$$\overline{\mathbf{N}}_{\mathbf{0}} = \begin{bmatrix} \frac{1215}{512} & -\frac{273}{128} & \frac{483}{512} & \frac{45}{456} \\ -\frac{95}{64} & \frac{833}{512} & -\frac{301}{256} & \frac{833}{512} & \frac{95}{642} \\ \frac{265}{512} & -\frac{301}{256} & \frac{833}{512} & \frac{95}{642} \\ \frac{45}{256} & \frac{483}{512} & -\frac{273}{139} & \frac{512}{512} \\ \frac{45}{256} & \frac{483}{512} & -\frac{273}{139} & \frac{512}{512} \\ \frac{45}{256} & \frac{483}{512} & -\frac{273}{139} & \frac{5125}{512} \\ \frac{45}{266} & \frac{483}{512} & -\frac{273}{139} & \frac{483}{512} \\ \frac{45}{266} &$$

For the first element:

$$\frac{\partial}{\partial x} \begin{bmatrix} f_{00} \\ f_{01} \\ f_{02} \end{bmatrix} = \frac{2}{h_0} \left(\overline{\mathbf{M}}_{\mathbf{10}}^{\alpha} + \overline{\mathbf{M}}_{\mathbf{20}}^{\alpha} \right) \begin{bmatrix} f_{00} \\ f_{01} \\ f_{02} \end{bmatrix} + \frac{2}{h_0} \overline{\mathbf{M}}_{+}^{\alpha} \begin{bmatrix} f_{10} \\ f_{11} \\ f_{12} \\ f_{13} \end{bmatrix} + \frac{2}{h_0} \theta \lambda \left(\overline{\mathbf{M}}_{\mathbf{10}}^{\alpha} + \overline{\mathbf{M}}_{\mathbf{20}}^{\alpha} \right) \begin{bmatrix} u_{00} \\ u_{01} \\ u_{02} \end{bmatrix} - \frac{2}{h_0} \theta \lambda \overline{\mathbf{M}}_{+}^{\alpha} \begin{bmatrix} u_{10} \\ u_{11} \\ u_{12} \\ u_{13} \end{bmatrix}$$

$$(D.2)$$

$$\overline{\mathbf{M}}_{\mathbf{10}}^{\alpha} = \begin{bmatrix} -\frac{9}{4} & 0 & 0\\ \frac{3}{20} & 0 & 0\\ \frac{3}{20} & 0 & 0 \end{bmatrix}, \quad \overline{\mathbf{M}}_{\mathbf{20}}^{\alpha} = \begin{bmatrix} \frac{3}{32} & \frac{55}{16} & -\frac{65}{32}\\ -\frac{97}{160} & -\frac{9}{16} & \frac{47}{32}\\ \frac{31}{160} & -\frac{25}{16} & \frac{15}{32} \end{bmatrix}$$

$$\overline{\mathbf{N}}_{\mathbf{0}}^{\alpha} = \begin{bmatrix} \frac{81}{32} & -\frac{15}{16} & \frac{45}{32} \\ -\frac{51}{160} & \frac{9}{16} & -\frac{27}{32} \\ \frac{21}{160} & -\frac{15}{16} & \frac{45}{32} \end{bmatrix}, \quad \overline{\mathbf{M}}_{+}^{\alpha} = \begin{bmatrix} \frac{105}{64} & -\frac{105}{64} & \frac{63}{64} & -\frac{15}{64} \\ -\frac{63}{64} & \frac{63}{64} & -\frac{189}{320} & \frac{9}{64} \\ \frac{105}{160} & -\frac{105}{160} & \frac{63}{64} & -\frac{15}{64} \end{bmatrix}$$

For the second element, the 3rd order flux scheme:

$$\frac{\partial}{\partial x} \begin{bmatrix} f_{10} \\ f_{11} \\ f_{12} \\ f_{13} \end{bmatrix} = \frac{2}{h_{1}} \overline{\mathbf{M}}_{-}^{\beta} \begin{bmatrix} f_{00} \\ f_{01} \\ f_{02} \end{bmatrix} + \frac{2}{\mathbf{h}_{1}} \overline{\mathbf{M}}_{0}^{\beta} \begin{bmatrix} f_{10} \\ f_{11} \\ f_{12} \\ f_{13} \end{bmatrix} + \frac{2}{\mathbf{h}_{1}} \overline{\mathbf{M}}_{+}^{\beta} \begin{bmatrix} f_{20} \\ f_{21} \\ f_{22} \\ f_{23} \end{bmatrix} + \frac{2}{\mathbf{h}_{1}} \theta \lambda \overline{\mathbf{M}}_{-}^{\beta} \begin{bmatrix} u_{00} \\ u_{01} \\ u_{02} \end{bmatrix} + \frac{2}{\mathbf{h}_{1}} \theta \lambda \overline{\mathbf{N}}_{0}^{\beta} \begin{bmatrix} u_{10} \\ u_{11} \\ u_{12} \\ u_{13} \end{bmatrix} - \frac{2}{\mathbf{h}_{1}} \theta \lambda \overline{\mathbf{M}}_{+}^{\beta} \begin{bmatrix} u_{20} \\ u_{21} \\ u_{22} \\ u_{23} \end{bmatrix}$$
(D.3)

$$\overline{\mathbf{M}}_{-}^{\beta} = \begin{bmatrix} \frac{1719}{4096} & \frac{2865}{2048} & -\frac{8595}{4096} \\ \frac{1011}{4096} & -\frac{1685}{2048} & \frac{5055}{4096} \\ -\frac{219}{4096} & \frac{365}{2048} & -\frac{1095}{4096} \\ -\frac{369}{4096} & \frac{615}{2048} & -\frac{1845}{4096} \end{bmatrix}, \quad \overline{\mathbf{M}}_{\mathbf{0}}^{\beta} = \begin{bmatrix} -\frac{14051}{12288} & \frac{1325}{4096} & \frac{4119}{4096} & -\frac{2563}{4096} \\ -\frac{25337}{12288} & \frac{1035}{4096} & \frac{5931}{4096} & -\frac{5931}{12288} \\ \frac{5401}{12288} & -\frac{5931}{4096} & -\frac{1035}{4096} & \frac{25337}{12288} \\ \frac{2563}{12288} & \frac{4119}{4096} & -\frac{13257}{4096} & \frac{14051}{12288} \end{bmatrix}$$

$$\overline{\mathbf{N_0^{\beta}}} = \begin{bmatrix} \frac{1215}{512} & -\frac{2/3}{128} & \frac{483}{512} & \frac{49}{256} \\ -\frac{95}{64} & \frac{833}{512} & -\frac{301}{256} & \frac{255}{512} \\ \frac{265}{512} & -\frac{301}{256} & \frac{833}{512} & -\frac{95}{64} \\ \frac{45}{256} & \frac{483}{512} & -\frac{273}{128} & \frac{1215}{512} \end{bmatrix}, \quad \overline{\mathbf{M}_+^{\beta}} = \begin{bmatrix} \frac{4305}{8192} & \frac{4305}{8192} & \frac{2833}{8192} & -\frac{615}{8192} \\ \frac{2555}{8192} & -\frac{2555}{8192} & \frac{1533}{8192} & -\frac{365}{8192} \\ -\frac{11795}{8192} & \frac{11795}{8192} & -\frac{7077}{8192} & \frac{1685}{8192} \\ \frac{20055}{8192} & -\frac{20055}{8192} & \frac{20035}{8192} & \frac{2865}{8192} \end{bmatrix}$$

Appendix E. Grid Structure II, boundary closure, last two elements

For the last two elements we make use of the following relationships. Define W^* for a matrix as:

$$W^* = \begin{bmatrix} -i & -h & -g \\ -f & -e & -d \\ -c & -b & -a \end{bmatrix}, \quad \text{where } W = \begin{bmatrix} a & b & c \\ d & e & f \\ g & h & i \end{bmatrix}$$
 (E.1)

For the (N-1)th element:

$$\frac{\partial}{\partial x} \begin{bmatrix} u_{(N-1)0} \\ u_{(N-1)1} \\ u_{(N-1)2} \\ u_{(N-1)3} \\ u_{(N-1)4} \end{bmatrix} = \frac{2}{h_{N-1}} \left(1 + \theta \frac{|a|}{a} \right) \overline{\mathbf{M}}_{-}^{\psi} \begin{bmatrix} u_{(N-2)0} \\ u_{(N-2)1} \\ u_{(N-2)2} \\ u_{(N-2)3} \end{bmatrix} + \frac{2}{\mathbf{h}_{N-1}} \left(\overline{\mathbf{M}}_{\mathbf{0}}^{\psi} - \theta \frac{|\mathbf{a}|}{\mathbf{a}} \overline{\mathbf{N}}_{\mathbf{0}}^{\psi} \right) \begin{bmatrix} u_{(N-1)0} \\ u_{(N-1)1} \\ u_{(N-1)2} \\ u_{(N-1)3} \\ u_{(N-1)4} \end{bmatrix} + \frac{2}{\mathbf{h}_{N-1}} \left(\mathbf{1} - \theta \frac{|\mathbf{a}|}{\mathbf{a}} \right) \overline{\mathbf{M}}_{+}^{\psi} \begin{bmatrix} u_{N0} \\ u_{N1} \\ u_{N2} \\ u_{N3} \\ u_{N4} \end{bmatrix}$$
(E.2)

where

$$\overline{\mathbf{M}}_{-}^{\psi} = (\overline{\mathbf{M}}_{+}^{\beta})^{*}, \quad \overline{\mathbf{M}}_{\mathbf{0}}^{\psi} = (\overline{\mathbf{M}}_{\mathbf{0}}^{\beta})^{*}, \quad \overline{\mathbf{N}}_{\mathbf{0}}^{\psi} = (\overline{\mathbf{N}}_{\mathbf{0}}^{\beta})^{*}, \quad \overline{\mathbf{M}}_{+}^{\psi} = (\overline{\mathbf{M}}_{-}^{\beta})^{*}$$

and for the Nth element:

$$\frac{\partial}{\partial x} \begin{bmatrix} u_{N0} \\ u_{N1} \\ u_{N2} \\ u_{N3} \end{bmatrix} = \frac{2}{h_N} \left(1 + \theta \frac{|a|}{a} \right) \overline{\mathbf{M}}_{-}^{\omega} \begin{bmatrix} u_{(N-1)0} \\ u_{(N-1)1} \\ u_{(N-1)2} \\ u_{(N-1)3} \\ u_{(N-1)4} \end{bmatrix} + \frac{2}{\mathbf{h}_N} \left(\left(1 - \theta \frac{|\mathbf{a}|}{\mathbf{a}} \right) \overline{\mathbf{M}}_{\mathbf{10}}^{\omega} + \overline{\mathbf{M}}_{\mathbf{20}}^{\omega} - \theta \frac{|\mathbf{a}|}{\mathbf{a}} \overline{\mathbf{N}}_{\mathbf{0}}^{\omega} \right) \begin{bmatrix} u_{N0} \\ u_{N1} \\ u_{N2} \\ u_{N3} \end{bmatrix}$$
(E.3)

where

$$\overline{\boldsymbol{M}}_{-}^{\omega} = \left(\overline{\boldsymbol{M}}_{+}^{\alpha}\right)^{*}, \quad \overline{\boldsymbol{M}}_{\boldsymbol{10}}^{\omega} = \left(\overline{\boldsymbol{M}}_{\boldsymbol{10}}^{\alpha}\right)^{*}, \quad \overline{\boldsymbol{M}}_{\boldsymbol{20}}^{\omega} = \left(\overline{\boldsymbol{M}}_{\boldsymbol{20}}^{\alpha}\right)^{*}, \quad \overline{\boldsymbol{N}}_{\boldsymbol{0}}^{\omega} = \left(\overline{\boldsymbol{N}}_{\boldsymbol{0}}^{\alpha}\right)^{*}$$

References

- [1] K. Van den Abeele, C. Lacor, Z.J. Wang, On the connection between the spectral volume and the spectral difference method, Journal of Computational Physics 227 (2) (2007) 877–885.
- [2] S. Adjerid, M. Aiffa, J.É. Flaherty, High-order finite element methods for singularly perturbed elliptic and parabolic problems, SIAM Journal Applied Mathematics 55 (2) (1995) 520–543.
- [3] S. Adjerid, K.D. Devine, J.E. Flaherty, L. Krivodonova, A posteriori error estimation for discontionuous Galerkin solutions of hyperbolic problems, Computer Methods in Applied Mechanics and Engineering 191 (2002) 1097–1112.
- [4] M. Ainsworth, Dispersive and dissipative behaviour of high order discontinuous Galerkin finite element methods, Journal of Computational Physics 198 (1) (2004) 106–130.
- [5] G. Ashcroft, X. Zhang, Optimized prefactored compact schemes, Journal of Computational Physics 190 (2) (2003) 459–477.
- [6] H. Atkins, C.-W. Shu, Quadrature-free implementation of discontinous Galerkin methods for hyperbolic egations, AIAA Journal 36 (775) (1998).
- [7] F. Bassi, S. Rebay, A high-order accurate discontinous finite element method for the numerical method for the numerical solution of the compressible Navier–Stokes equation, Journal of Computational Physics 131 (267) (1997).
- [8] K.S. Bey, J.T. Oden, A Runge–Kutta discontinuous Galerkin finite element method for high speed flows, in: 10th AIAA Computational Fluid Dynamics Conference, Honolulu, Hawaii, 1991, pp. 24–27.
- [9] R. Biswas, K.D. Devine, J. Flaherty, Parallel adaptive finite element methods for conservation laws, Applied Numerical Mathematics 14 (1994) 255–283.
- [10] J.P. Boyd, Chebychev and Fourier Spectral Methods, second ed., Dover, Minneola, New York, 2000, pp. 86, 98–108, 570.
- [11] M.H. Carpenter, D. Gottlieb, S. Abarbanel, The stability of numerical boundary treatments for compact high-order finite-difference schemes, Journal of Computational Physics 108 (1993) 272–295.
- [12] B. Cockburn, C.-W. Shu, TVB Runge–Kutta local projection discontinuous Galerkin finite element for conservation laws II. General framework, Mathematical Computing 52 (411) (1989).
- [13] B. Cockburn, S.Y. Lin, C.-W. Shu, TVB Runge-Kutta local projection discontious Galerkin finite element for conservation laws III. One dimensional systems, Journal of Computational Physics 84 (90) (1989).
- [14] B. Cockburn, G.E. Karniadakis, C.-W. Shu, The development of discontinous Galerkin methods, Lecture Notes in Computational Science and Engineering, or in: B. Cockburn et al. (Ed.), Discontinous Galerkin Methods, Springer-Verlag, Berlin, 2000, p. 3.
- [15] B. Cockburn, C.-W. Shu, The Runge–Kutta discontinuous Galerkin method for the conservation laws, V, Journal of Computational Physics 141 (1998) 199–224.
- [16] B. Cockburn, Devising discontinous Galerkin methods for non-linear hyperbolic conservation laws, Journal of Computational and Applied Mathematics 128 (2001) 187–204.
- [17] A.M. Fernando, F.Q. Hu, A finite difference scheme based on the discontinous Galerkin method applied to wave propagation, AIAA Paper, 2008, pp. 2008–2874.
- [18] J.E. Flaherty, L. Krivodonova, J.-F. Remacle, M.S. Shephard, Aspects of discontinous Galerkin methods for hyperbolic conservation laws, Finite Elements in Analysis and Design 38 (2002) 889–908.
- [19] T. Hagstrom, J. Goodrich, I. Nazarov, C. Dodson, High-order methods and boundary conditions for simulating subsonic flows, AIAA Paper, 2005, pp. 2005–2869.
- [20] R. Hixon, Prefactored small-stencil compact schemes, Journal of Computational Physics 165 (2000) 522-541.
- [21] F.Q. Hu, M.Y. Hussaini, J.L. Manthey, Low dissipation and low dispersion Runge Kutta schemes for computational acoustics, Journal of Computational Physics 124 (1996) 177–191.

- [22] F.Q. Hu, M.Y. Hussaini, P. Rasetarinera, An analysis of the discontinuous Galerkin method for wave propagation problems, Journal of Computational Physics 151 (1999) 921–946.
- [23] F.Q. Hu, A stable, perfectly matched layer for linearized Euler equations in unsplit physical variables, Journal of Computational Physics 173 (2001) 455–480.
- [24] F.Q. Hu, H.L. Atkins, Eigensolution analysis of discontinuous Galerkin method. Part I: One space dimension, Journal of Computational Physics 182 (2002) 516–545.
- [25] F.Q. Hu, X.D. Li, D.K. Lin, Absorbing boundary conditions for nonlinear Euler and Navier–Stokes equations based on the perfectly matched layer technique, Journal of Computational Physics 227 (2008) 4398–4424.
- [26] S.K. Lele, Compact finite difference schemes with spectral-like resolution, Journal of Compututational Physics 103 (1992) 16–24.
- [27] P. Lesaint, P.A. Raviart, On a finite element method for solving the neutron transport equation, Mathematical Aspects of Finite Elements in Partial Differential Equations, Academic Press, San Diego, 1974. pp. 89–145.
- [28] Y. Liu, M. Vinokur, Z.J. Wang, Spectral difference method for unstructured grids. I: Basic formulation, Journal of Computational Physics 216 (2006) 780–801.
- [29] E. Marchendise, N. Chevaugeon, J.-F. Remacle, Spatial and spectral superconvergence of discontinuous Galerkin method for hyperbolic problems, Journal of Computation and Applied Mathematics 215 (2008) 484–494.
- [30] M. Popescu, W. Shyy, M. Garbey, Finite volume treatment of dispersion-relation-preserving and optimized prefactored compact schemes for wave propagation, Journal of Computational Physics 103 (2005) 705–729.
- [31] W.H. Reed, T.R. Hill, Triangular Mesh Methods for the Neutron Transport Equation, Los Alamos Scientific Laboratory Report LA-UR-73-479, 1973.
- [32] C.K.W. Tam, J.C. Webb, Dispersion-relation-preserving schemes for computational acoustics, Journal of Computational Physics 107 (1993) 262-281.
- [33] Z.J. Wang, Spectral (finite) volume methods for conservation laws on unstructured grids, Journal of Computational Physics 178 (2002) 210-251.
- [34] M. Zhang, C.-W. Wang, An analysis of and a comparison between the discontinuous Galerkin and the spectral finte volume methods, Computers & Fluids 34 (2005) 581–592.